Response of the HI-STORM Spent Nuclear Fuel Storage Cask to a Large Explosive Charge Blast

REDACTED

02/12/2008

Document 2

The Nuclear Regulatory Commission does not support many of the assumptions and/or information contained in this report. This report cannot be used independently to develop any conclusions regarding security or protective measures. This report should not be shared with industry and should not be released to anyone outside the agency.

Response of the HI-STORM Spent Nuclear Fuel Storage Cask to a Large Explosive Charge Blast (U)

Marlin E. Kipp, Jeremy Sprung, Doug Ammerman, Jeffrey Smith, Ken Sorenson
Sandia National Laboratories
Albuquerque, New Mexico 87185-07188

August 22, 2004

Abstract (U)

(U) Numerical simulations are described that evaluate the consequences of an explosive blast load on the HI-STORM spent fuel rod storage cask. Detailed models of the HI-STORM concrete storage cask and MPC-24 fuel assembly canister have been assembled for analyses using the three-dimensional Eulerian shock wave propagation code, CTH.

ex. 2

p. 1a

CLASSIFIED BY:	Ken B. Sorenson
TITLE/ORG:	Manager 6141/August 18, 2005
DERIVED FROM:	CG-RDM-1, June 1996 and CG-NMF-2, Dec 1991
DECLASSIFY ON:	X4

~~CONFIDENTIAL~~

This Page Intentionally Left Blank

Acknowledgements (U)

(U) The authors gratefully acknowledge the support of R. J. Kalan and R. H. Yoshimura, Sandia National Laboratories, during this study, who provided the necessary drawings and consultation required to make the analyses possible. Frequent conversations with G. C. Bessette, Sandia National Laboratories, over the course of this work also proved most helpful.

Table of Contents (U)

ex 2 p 4a

ex 3 p 4k

List of Figures (U)

S C1
Ex 3
p 5a

~~CONFIDENTIAL~~

Ex # 2 p.6a

List of Tables (U)

Ex 2 aaa-SR1 p. 7a

Response of the HI-STORM Spent Nuclear Fuel Storage Cask to a Large Explosive Charge Blast (U)

Executive Summary (U)

(U) The events of September 11th, 2001 have led to the need to evaluate radioactive material storage and transportation casks for threats from sabotage. The U.S. Nuclear Regulatory Commission (NRC) contracted Sandia National Laboratories to conduct the following study to evaluate the response of a Holtec HI-STORM 100 Cask System to a large blast sabotage event. The amount of explosive and standoff distance is representative of a scenario of a small truck parked directly adjacent to the cask. The scenario parameters for this event were defined by NRC design basis threat criteria and by NRC staff, where more specifity was required to define the event. This loading simulates a truck delivery of the explosive, parked adjacent to the cask. EX1 8a

(U) Numerical simulations are described that evaluate the consequences of an explosive blast load on the HI-STORM storage cask. The steel structure and unreinforced concrete fill of this storage cask were modeled in substantial detail. Each fuel rod assembly in the MPC-24 structure was modeled as a mass of homogeneous material: the effective empty space in each assembly was uniformly distributed through its enveloped volume, resulting in an averaged reduced density relative to that of the solid fuel, and represented with a porous material model. The 24 fuel assemblies were included in a model of the support structure within the canister, and the canister located on the pedestal inside the storage cask. The numerical analyses used the three-dimensional Eulerian shock wave propagation code, CTH, to simulate the detonation of the explosive charge and subsequent interaction with the cask. EX3 8b p.8b

(U)

DUO-SR1
EX 2
p. 9a

The canister inventory of radionuclides significant for radiological health effects was constructed from the results of an ORIGEN calculation for an 8x8 fuel BWR assembly that had been cooling for ten years.

Ex-3 p. 9b

Ex. 2
DUO-SR1
p. 9c

DUO-SR1
p. 9d Ex 2

(U)

(U)

DUO-SR1
p. 9e
Ex 2

OJO-SR
EX 2
p. 10a

(U)

This Page Intentionally Left Blank

Response of the HI-STORM Spent Nuclear Fuel Storage Cask to a Large Explosive Charge Blast (U)

1 Introduction (U)

(U) The events of September 11th, 2001 have led to the need to evaluate radioactive material storage and transportation casks for threats from sabotage. The U.S. Nuclear Regulatory Commission (NRC) contracted Sandia National Laboratories (SNL) to conduct the following study to evaluate the response of a Holtec HI-STORM 100 Cask System (HI-STORM) to a large blast sabotage event.

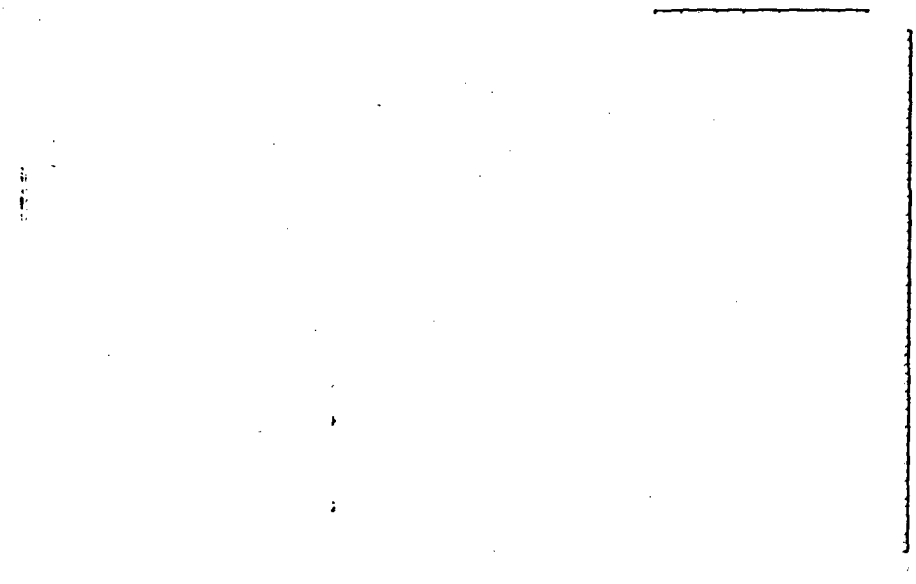

Figure 1-1. The Threat: Cask, Truck, and Explosive Layout (U).
The contents of this figure are unclassified.

(U) The numerical analysis approach taken here is similar to that reported for the NAC-UMS and NLI-1/2 fuel transportation casks (Kipp, 2004). A detailed model of this cask was constructed, along with the appropriate fuel assembly inside the cask (24 element MPC fuel basket assembly). The goal of the blast analyses was to assess the consequences to the cask, canister, and fuel, including whether breach would occur, and estimate the damage imparted to the fuel elements. This information could then be used to estimate the potential formation and release of radiological aerosols from the cask that would in turn define a source term for regional dispersal.

CNSI Ex 1 p13a

(U) One uncertain aspect of the analyses reported here is the determination of a definitive threshold for breaching the fuel container and assessing fuel rod damage. When the loading conditions are either significantly less than or far in excess of a threshold, then the task is relatively straightforward. Near the threshold, it is much more difficult to make a precise determination of whether breaching of the containment vessel will occur, the size of any holes that might be formed leading from the outside to the interior of the casks, and whether the fuel

itself has been damaged adequately to be released even if breaching has been successful. In the present study, a visual assessment was the primary means to glean from the analyses an evaluation of potential breaching. For the assessment of fuel state, reference can be made to previous studies in which low velocity impacts clearly led to aerosols formed (*e.g.*, Kass, 1985). Critical energy density in the fuel is also cited as a means to assess aerosol formation (*e.g.*, Sandoval, 1984), but still requires establishing a clear path to exit the cask. Aspects of determining an appropriate energy density for the homogeneous fuel assembly model are discussed in Appendix C.

(U) It should also be noted that, although some attempt was made to include lid details and accompanying retaining bolts, determining whether or not the lid will be broken open at very late times (e.g. secondary impact) is not within the capabilities of the code. Were the loading so extreme as to cause large internal pressures that push open the lid, there is a possibility that these analyses would reveal such behavior.

14a
EX2
DUO-S21

The canister inventory of radionuclides significant for radiological health effects was constructed from the results of an ORIGEN calculation for an 8x8 fuel BWR assembly that had been cooling for ten years.

14b
EX 3
SG1

000-SR1
Ex 2
p. 15a

~~CONFIDENTIAL~~

2 Hi-Storm Cask Geometry, Model, And Material Definition (U)

(U) This section describes the HI-STORM cask geometry model, as well as limited ancillary structural members associated with the cask. As noted in the Introduction, all the modeling is done with the CTH shock wave propagation code; a three-dimensional rectilinear space is defined with a specified cell size (not necessarily uniform), and the constituent parts are inserted into this mesh with a sequence of basic geometry definition packages. Since the constructed cask model is independent of the mesh definition, modification of the numerical resolution requires only alteration of the mesh cell dimensions. Numerical resolution effects are included in the discussion of the cask analyses in the subsequent section.

(U) The HI-STORM storage cask included a 24-element MPC fuel basket assembly as a representative canister filled with spent nuclear fuel rods. For this large storage cask, evaluation of site constraints concluded that the nearest reasonable placement of explosive would be 0.3 m (1 ft) from the vertical surface of the cask (0.3 m (1 ft) from the surface of the charge to the surface of the cask). The position of the lower face of the charge above the concrete pad was defined to be 1 m (3 ft), an approximate truck bed height. Appropriate material properties were utilized to represent the components (see Appendix A). The large dimensional scale of the cask and explosive charge severely limit the level of detail (resolution) that can be accommodated in these simulations. As noted previously, in the Eulerian structure of CTH, material interfaces are defined only to within a cell dimension. Spatial features significantly less than this dimension can be inserted into the computational mesh, but become part of the mass in a mixed material cell (cell with multiple materials), losing their distinctive character. However, should there be a possibility of subsequent simulations with finer resolution, then there is no penalty for including the finely detailed geometry definition. However, some components (cladding on individual fuel pellets, for example) have dimensions significantly less than any expected cell size, and were not modeled.

(U) For the fuel rod assemblies, an average density was determined for an individual fuel element assembly tube, and then representative properties were assigned to this unit. The average density of the fuel assembly was determined to be approximately 5.1 g/cm^3 (316.2 lb/ft^3). Each of the 24 fuel assemblies (22.05 cm (8.681 in) square by 448.3 cm (176.5 in) tall) was treated as a homogeneous porous material, with this average reference density of 5.1 g/cm^3, from which the void volume (free volume within the unit) could be decreased as the material is compressed. When the void volume is fully removed, the material then responds with the fully dense uranium oxide behavior. The solid density of the fuel was taken to be that of uranium dioxide – about 10.3 g/cm^3 (638.6 lb/ft^3). This approach permits the fuel to respond nominally as if the full definition of the fuel were included, although any contribution of cladding was not included in this material approximation. For shock propagation purposes, this model serves to approximate the crush behavior of the fuel assembly. Where the details of individual fuel rod response required, a more precise definition of the fuel cladding and individual components could be inserted into the mesh, but the requisite refinement in numerical resolution and computational demands is well beyond what current platforms can provide. Such level of detail is reserved for analyses of smaller, more localized regions of interest (*e.g.*, contact charges on fuel assemblies).

(U) All of the computational region not occupied by cask and explosive charge was filled with ambient air (1 atmosphere, or about 101.4 kPa (14.7 psi), at an initial density of 0.001 g/cm^3 (0.062 lb/ft^3)).

(U) The model for the HI-STORM cask was derived from drawings in the HI-STORM Topical Safety Analysis Report (Holtec International, 2000). An exterior view of the cask model, pad, with the explosive charge is shown in Figure 2-1

17a Ex2
000-SR1

The pedestal at the base, the concrete sections comprising the lid, and the steel radial stiffeners embedded in the main concrete wall can be seen in Figures 2-2 and 2-3.

(U) There are four cooling ports at the top and bottom of the cask, some of which are visible in Figure 2-1. The total height of the cask is 608.33 cm (239.5 in; or 19.96 ft). The MPC-24 fuel basket assembly, in its canister, has been inserted into this cask, resting on the pedestal, and centered axially (*cf.* Figure 2-3).

17b Ex2
000-SR1

The overall mass of the HI-STORM storage cask model is 111 Mg (122.4 tons); the canister and MPC-24 basket assembly model with a complete fuel load has a mass of 44 Mg (48.5 tons). The combined model mass of overpack and canister is 155 Mg (171 tons).

17c Ex3
SG1

Figure 2-1. Exterior view of the HI-STORM storage cask, concrete pad and explosive charge (U).

The contents of this figure are unclassified.

18a Ex3
SGI

Figure 2-2. Interior section view of the HI-STORM storage cask with the MPC-24 fuel basket assembly resting on the pedestal (U).

The contents of this figure are unclassified.

(U) The computational space into which this container and explosive were inserted spanned 8 m (26.25 ft) through the explosive-cask direction; 6 m (19.7 ft) transverse to the explosive, and 8 m (26.25 ft) along the axes of the cask. This gives ample space for the explosive products to expand and exit the mesh, and to accommodate the limited motion of the container for the time duration of the simulation. Uniform spatial resolution of 2.5 cm (1 in) requires 24.6 million cells, and a simulation with key regions in the vicinity of the explosive of 1.5 cm (0.6 in) resolution required 31.2 million cells. The simuation timestep is basically a currant evaluation (cell dimension divided by sound speed). The very minimum resolution that was expected to be accessible was 1.5 cm (0.6 in), with 2.5 or 5 cm (1.0 or 2.0 in) also used for preliminary simulations. Under such limitations, the outer shells of the cask and MPC have insufficient cells to be resolved, and were shown to provide inadequate confinement during loading by the explosive products and accompanying blast wave (Appendix B) (that is, with inadequate number of cells through the shell thickness, it becomes circumferentially discontinuous, and cannot support hoop loads). To counter this effect, the external steel layer was "fluffed" to a thickness of 10 cm (3.9 in), to be at least several cell widths, retaining the outer diameter of the original shell. This modification was done in such a way as to approximately preserve the shell and displaced concrete mass (replacing the steel with aluminum), and reducing the yield strength of the shell so that the original circumferential strength (yield strength times the cross sectional area) was maintained. Similar expansion of the MPC canister wall outwards (to 7 cm (2.8 in)) was made for the same reason (Appendix B), requiring that the U-shaped spacers be removed

from the inner surface of the cask to accommodate this increased diameter. In this case, an artificial density of the exterior wall of 1.40 g/cm^3 (86.8 lb/ft^3) was required. The thickened shells of the cask and canister are apparent in Figures 2-2 and 2-3, and may be contrasted to the original wall thicknesses that appear in the figures in Appendix B.

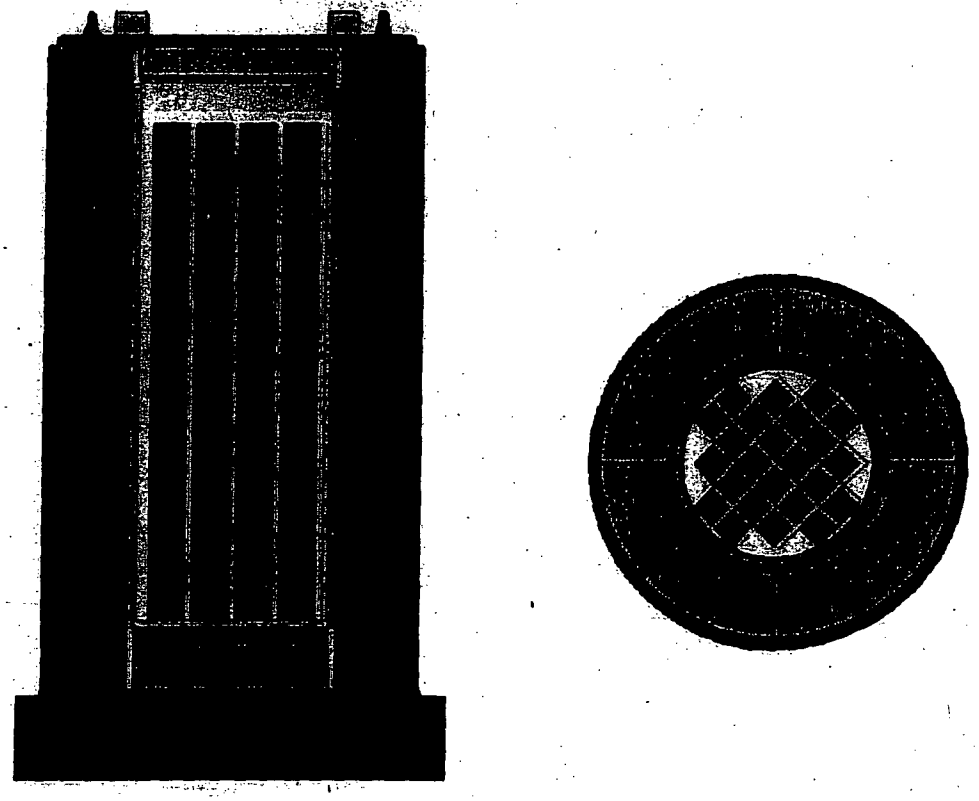

Figure 2-3. Longitudinal cross-section view of the HI-STORM storage cask (left) and transverse view of the central region of the cask with the MPC-24 fuel basket assembly (right) (U).

The contents of this figure are unclassified.

Ex 1
CNSI
19a

EX 3
p. 20a

Figure 2-4. Longitudinal section view of the HI-STORM cask and the charge (U).
The contents of this figure are unclassified.

EX 3
p. 20 b

Figure 2-5. Transverse section views of the HI-STORM cask and the charge: Cask radial stiffener orientation relative to the explosive charge 45° (left) and 0° (right) (U).
The contents of this figure are unclassified.

3 Hi-Storm Cask Response To a TNT Explosive Charge (U)

3.1 Blast Calculations (U)

(U) Consequences of insults to the HI-STORM cask by the explosive charge are reported in this section. The charge configuration is limited to a bare TNT charge in close proximity to the cask. The user-defined flags which must be set in the code that define yield and fracture properties in cells with more than one material were discussed in Appendices C and D of Kipp (2004). As noted in those appendices, the mixed cell fracture and yield are critical parameters. The mixed cell fracture needs to be set to a large enough negative number so that when explosive products share the same cells as steel (or other exterior shell material), the cell fracture stress is nominally that of steel. This ensures that the steel surfaces retain their full strength.. It was also found that the mixed cell yield option had to be set so cells with multiple materials were assigned a yield stress calculated from the volume-weighted yields of the individual constituent materials. The other cause for ablation – minimal resolution of a thin shell – has been moderated by the use of fluffed layers, as discussed in the previous section and Appendix B. As noted in the previous section, two orientations of the cask radial stiffeners relative to the explosive charge were examined in order to determine if there were any significant differences in the response of the cask and internal loads transmitted to the MPC.

3.2 Cask Orientation 45° (Charge Midway Between Radial Stiffeners) (U)

(U) The face of this explosive charge is centered along the axis of the cask, midway between two of the radial steel stiffeners

P21a
SG1
Ex3

SG1
P21b
Ex3

The inset indicates the pressure history on the cask surface directly in line with the charge centerline.

P21c
000-SR4
Ex 2

delete

EX3
p. 22a

EX2
p. 22b

SGI
EX 3
p. 23a

Ex. #2
p. 23b

Ex 3
p.24a

Ex #2
p. 24b

Ex 3
p. 24 c

Ex #2
p. 24d

(U) The pressure pulse on the cask directly under the charge is basically unloaded by 0.6 ms (see inset in Figure 3-1), but the peak pressures on the more distant regions of the cask surface are not fully unloaded until nearly 2 ms have elapsed. The peak pressure *vs.* distance along the cask is plotted in Figure 3-5, clearly showing that the maximum incident pressures are located directly under the charge. The peak pressures fall off rapidly away from the charge towards the base and upper ends of the cask. Although the incident pressure on the cask is unloaded by 2 ms, there ensues a long 'coasting' period in which the locally induced deformations are transmitted through the cask, coupling motion of the exterior structure and interior components, leading eventually to general cask translation. In the time frame of this simulation (16 ms), though, the actual displacement of the cask is minimal.

25a
Ex 2
OUO-SRI

25b
Ex 3
SGI

Figure 3-5. Peak incident pressure on the surface of the HI-STORM storage cask as a function of axial distance along the cask for the TNT charge (1 ksi = 6.895 MPa; 1 m = 3.28 ft) (U).

The contents of this figure are unclassified.

SGI EX 3
p 26a

Figure 3-6. Average velocity history of the concrete and fuel in the HI-STORM storage cask (1 m/s = 2.24 mph) (U).

The contents of this figure are unclassified.

(U) Because the charge is located eccentrically relative to the center of mass of the cask, there is a velocity gradient created along the axis of the cask whose magnitude varies over time until equilibrium is attained.

Ex #2
p. 26b

Subsequent sliding motion of the cask is not explicitly treated in this analysis.

EX 3
p. 27a

Figure 3-7. Velocity histories of two points in the cask separated by 4 m (13.1 ft): one near the cask bottom (solid), and one near the cask top (dashed) (1 m/s = 2.24 mph; 1 m = 3.28 ft) (U).

The contents of this figure are unclassified.

EX 3
p. 27b

Figure 3-8. Angular velocity determined from the velocities of the two points in Figure 3-7, which are separated by a distance of 4 m (13.1 ft) (U).

The contents of this figure are unclassified.

(U) The possibility for tipping can be approximately determined from the conditions where the translation velocity is interrupted by the bottom cask edge suddenly constrained to zero motion. Assuming the moving storage cask would acquire a rotational kinetic energy equivalent to its translational kinetic energy, comparison of that energy to the potential energy required to lift the center of mass to the highest point through the rotation provides a means to evaluate the potential for tipping.

(U)

P28a Ex2 000-SR1

P28b SG1 Ex3

3.3 Cask Orientation 0° (Charge Centered Over Radial Stiffeners) (U)

P28c 000-SR1 Ex2

SGI Ex 3
p. 29a

Ex. #2
p. 296

Ex 3
p. 29c
SGI

Ex 2
p. 29d

Ex
#2
p 29e

EX 3
p. 30a

e

EX 3
p. 30b

Ex. #2
p. 30c

Ex #2
p. 31a

EX 2
p. 31b

EX 2
p. 31c

Ex 3
p. 32a

Ex 2
p. 32b

The contents of this figure are unclassified.

(U)

Ex 3
p. 32c

Ex 3
p. 32d

Ex 2
~~Ex~~ p. 32e

4 Summary of Post-Blast Fuel Characteristics (U)

4.1 Fuel Response (U)

Ex #2
P33a

As noted in previous discussions, the fuel is represented as a homogeneous material with distributed void to account for the void distributed throughout the assembly volume.

Ex 3
P33b

To make the correlation between the homogeneous material and explicit fuel pellets, single pellet configurations have been calculated and the energy histories compared, as discussed in Appendix C.

(U) In the present case, the shock source is localized, and it is to be expected that these characteristics will vary as a function of position along the fuel rod assemblies. Monitoring points within the fuel assemblies (23 points distributed along the length of each assembly) provide local histories through the duration of the explosive event, and the peak values are extracted.

SG1
P33C
Ex 3

These massless history particles were located at 20 cm (7.9 in) spacing along the length of each assembly. The symmetry of the configuration requires evaluation of only one-half of the 24 assemblies. A numbering scheme for the assemblies in the simulation is shown by the schematic in Figure 4-1. These labels are used to identify the assemblies in subsequent plots. By associating a mass of the assembly with each tracer, a summary of the affected fuel can be assessed.

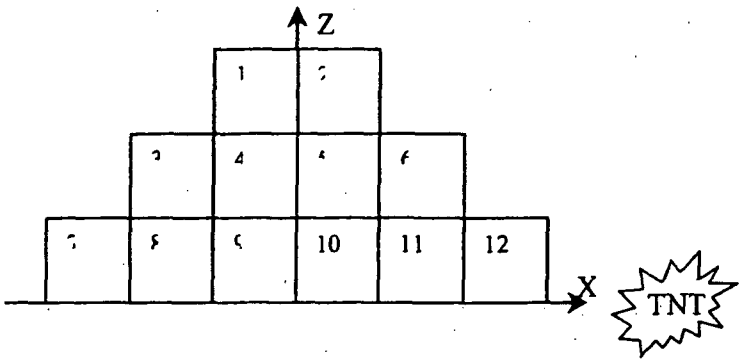

Figure 4-1. Numbering scheme for the fuel tubes. Only one-half of the array is shown, since the explosive charge is positioned on a plane of symmetry (U).
The contents of this figure are unclassified.

4.2 Assembly Accelerations (U)

SGI Ex 3 p. 34a

SGI Ex 3 p. 34b

SGI Ex 3 34c

Figure 4-2. Peak fuel accelerations in Assemblies 1 – 6 (1 cm/s^2 = 0.033 ft/s^2; 1 cm = 0.394 in) (U).

The contents of this figure are unclassified.

SG1
Ex3
P35a

Figure 4-3. Peak fuel accelerations in Assemblies 7 – 12. (1 cm/s^2 = 0.033 ft/s^2; 1 cm = 0.394 in) (U).

The contents of this figure are unclassified.

4.3 Assembly Internal Energy Amplitudes (U)

SG1
Ex3
P35b

Figures 4-4 and 4-5 summarize the energy density axial distributions for the TNT charge. Again, the largest amplitudes are located directly under the explosive charge. These energy densities are the result from the homogeneously distributed fuel model. As discussed in Appendix C, if the discrete nature of the individual fuel tubes is taken into account, the absorbed energy is reduced by a factor of 1.6.

Ex 3
p. 36a

Figure 4-4. Peak fuel internal energy in Assemblies 1 – 6 (1 J/g = 0.430 BTU/lb ; 1 cm =0.394 in) (U).

The contents of this figure are unclassified.

Ex 3
p. 36b

Figure 4-5. Peak fuel internal energy in Assemblies 7 – 12 (1 J/g = 0.430 BTU/lb ; 1 cm =0.394 in) (U).

The contents of this figure are unclassified.

EX 3
p. 37a

The energy density in this equation is the input energy in a Pellini Hammer test (the kinetic energy of the falling weight). The energy in figures 4-4 and 4-5 is an absorbed energy amount. Appendix C discusses a method for correlating internal energy to input energy for the Pellini Hammer tests. This method shows that only about 60% of the input energy is converted to internal energy in the fuel.

EX 3
p. 37b

EX 3
p. 37c

4.4 Assembly Temperature Rises (U)

SGI
EX 3
p. 37d

>CI

5 Discussion Of Blast Calculation Results (U)

(U) The simulations of the HI-STORM spent fuel storage cask response to a large explosive charge discussed in this report reflect the capabilities of current analysis code and computing platforms

Ex 2
p. 37a

(U) The fuel was represented as a homogeneous porous mixture within individual assemblies, based on the total mass of fuel present and the volume available. This was viewed, for the present types of loading, to be a suitable compromise in modeling, accepting that numerical resolution cannot meet the fine details of the individual fuel rods

EX2
p. 38b

Clamped

EX1
p. 38c

Ex 2
p. 38d

Improved resolution may provide additional insight into this potential penetration scenario.

SGI
p. 38e
EX 3

EX 3
SGI
p. 38f

SGI
EX 3
p. 39a

OUO-SRI
P40a
Ex 2

6

6.1 Event Definition (U)

P40b
OUO
Ex2

P40c
SG1
EX3

P40d
OUO
SRI
Ex2

P40e
SG1
EX3

EX1
P.40f

EX2
OUO
SRI
P.40g

EX3
S61
p. 41a

p41b
OWO-SR1
Ex2

6.2.1 Cask Inventory (U)

(U) ORIGEN ((Croff, 1980) and (ORNL, 1991)) was used to calculate the inventory of a single high-burnup (3.31% UO_2; 50,008 MWD/MTIHM,) BWR/6, 8x8 fuel assembly. Because an ORIGEN calculation provides output for over 800 radionuclides, the number of radionuclides in the ORIGEN output was reduced by dividing the 10-year cooled amount of each radionuclide by its A_2 value ((IAEA, 1987) and (CFR)) and then selecting the smallest set of these normalized curie amounts that yielded a sum greater than 99.9 percent of the sum of all of these normalized curie amounts. This procedure reduced the ORIGEN output set of over 800 radionuclides to a much smaller set of 19 radionuclides that are important for the estimation of radiological health effects. Table 6-1 lists these 19 radionuclides and gives the amount of each nuclide in Becquerels in one high-burnup, BWR/6, 8x8 ten-year cooled, spent fuel assembly.

Table 6-1. Radionuclide Inventory (Bq) of One High-Burnup, BWR/6, 8x8, Ten-Year Cooled, Spent Fuel Assembly (U)

The contents of this table are unclassified.

Nuclide	Amount (Bq)	Nuclide	Amount (Bq)	Nuclide	Amount (Bq)
Co-60	2.96E+11	Ce-144	7.47E+11	Am-241	1.77E+13
Kr-85	4.07E+13	Pm-147	4.96E+13	Am- 242m	2.90E+11
Sr-90	5.00E+14	Pu-238	5.85E+13	Am-243	4.51E+11
Y-90	5.00E+14	Pu-239	2.75E+12	Cm-242	2.39E+11
Ru-106	4.29E+12	Pu-240	5.11E+12	Cm-243	4.44E+11
Cs-134	7.55E+13	Pu-241	7.70E+14	Cm-244	8.33E+13
Cs-137	8.14E+14				

(U) Co-60 is formed by activation of Ni-60. Ni-60 is a constituent of Zircaloy, the alloy from which fuel rod cladding is fabricated, and also of the CRUD (Hazelton, 1987) deposits that form

on fuel rod cladding surfaces during reactor operation. Because release of Co-60 that is formed inside of Zircaloy fuel rod cladding can not occur, while Co-60 that is formed by activation of Ni-60 in CRUD can be released by spallation of these deposits from cladding surfaces, the Co-60 inventory calculated by ORIGEN for activation of Ni in cladding was replaced by an estimate of the amount of Co-60 in CRUD. This estimate was developed as follows. If the peak surface concentrations at discharge for average burnup fuel rods (Sandoval, et al, 1991[b]) are assumed to apply to the entire rod surface, then Co-60 discharge inventories for BWRs are about 64 Ci. If high-burnup fuel is in the reactor for 5 cycles and average burnup for 3 cycles, at discharge there will be 5/3 more CRUD on high-burnup rods than on average burnup rods. Further, decay will reduce Co-60 amounts by 0.5 during each successive 5-yr period. Lastly, measurements of the variation of CRUD layer thickness with position on spent fuel rods (Lukic and Schmidt, 2003) indicate that $d_{CRUD,Av}/d_{Crud,Max} = 0.3$. Thus,

$$\text{Co-60} = I_{discharge}(d_{CRUD,Av}/d_{CRUD,Max})(\text{burnup factor})(\text{decay factor})$$
$$= (64\ \text{Ci})(0.3)(5/3)(0.5)^2(3.7\text{x}10^{10}\ \text{Bq/Ci}) = 2.96\text{x}10^{11}\ \text{Bq}$$

(U) Lastly, in order to have a noble gas in the inventory, although eliminated by the A_2 screen, Kr-85, the noble gas with the largest curie amount in the ORIGEN inventory for 10-year cooled high burnup spent BWR fuel, was added back into the inventory using the amount calculated by ORIGEN.

SG1 P429 Ex3

[

SG1 429 Ex3

]

The scale factor used was the ratio of the peak acceleration experienced at each location along the length of the lumped mass that represented the rods in an assembly to the 100 G acceleration for which the strain map in Figure 6-1 was calculated.

Ex2 cont'd next page OUO-SGI p.42c

[1] Personal communication, C. Beyer. August 2003.

OUO-X4
EX2
p.43a

Figure 6-1. Peak Tensile Strains and Rod-to-Rod Pinch Forces for a 30 mph Side Impact of a Model of One 7x1 Slice of a GE 7x7 BWR Fuel Assembly (U)

The contents of this figure are unclassified.

OUO-SRI
EX2
p.43b

(U) **BWR Spent Fuel.** The HI-STORM Topical Safety Analysis Report (TSAR) (TSAR[d]) states that the free volume of a spent fuel rod in the 8x8 BWR assemblies is 1.235 in^3 = 20.2 cm^3 and the TN-68 SAR (Transnuclear Inc, 2000[a]) states that rods in 8x8 BWR assemblies have minimum free volumes that range from 20.9 to 26.1 cm^3. The TN-68 Safety Analysis Report (SAR) (Transnuclear Inc, 2000[b]) states that the mass of the stainless steel springs in the fuel rods in a single assembly is 1.05 kg. Since the density of stainless steel is 8.03 g/cm^3, the volume of one spring is about (1050 g/assembly)/(8.03 g/cm^3)(64 rods/assembly) = 2 cm^3. Reasonable values ((TSAR[b]), (Transnuclear Inc, 2000[c]), and Sanders et al, 1990[a]) for the length and i.d. of a BWR spent fuel rod, the active fuel length of the fuel pellets, and the pellet diameter are L_{rod} = 4.09 m, d_{rod} = 1.064 cm, $L_{pellets}$ = 12 ft = 366 cm, and d_{pellet} = 1.057 cm. Therefore, $V_{rod} = \pi(d_{rod}/2)^2 L_{rod} - \pi(d_{pellet}/2)^2 L_{pellets} - V_{spring}$ whereupon substitution of values for these parameters yields V_{rod} = 41 cm^3. Since the TN-68 SAR states that the V_{rod} values it lists for 8x8 BWR

assemblies, which range from 20.9 to 26.1 cm^3, are minimum values, it is here assumed that V_{rod} = 40 cm^3.

(U) **Spent Fuel Pellet Properties.** During reactor operation, compression of fuel cladding and swelling and cracking of the fuel pellets in a fuel rod largely eliminates the rod's fuel-cladding gap and creates an internal network of cracks inside of the pellets that has a free volume about equal to the volume of the fuel-cladding gap in fresh fuel. Abrasion during insertion of the pellets into the rod and vibration during reactor operation causes fuel fines to form on pellet external surfaces and also on pellet crack surfaces. In high-burnup spent fuel pellets, capture of epithermal neutrons by Uranium atoms in the pellet rim produces a friable layer of fuel fines on the outer surface of each pellet. Measurements indicate that the thickness of this friable rim layer in high burnup BWR spent fuel is about 150 μm ((Manzel and Walker, 2002), (Einziger and Beyer, 2004), and (Manzel and Walker, 2000)).

(U) Because the body and the rim of high burnup spent fuel pellets have quite different morphologies ((Manzel and Walker, 2002), (Thomas et al, 1992), and (Spino et al, 1996)), release of noble gases and of fuel fines from these two regions of a high burnup pellet will be quite different. Like fresh UO_2 pellets, the body regions of high burnup spent fuel pellets consist of sintered 10 μm UO_2 particles. The voids and the internal crack network that form in pellet bodies cause these body regions to have porosities of 5 to 10 percent ((Manzel and Walker, 2002), (Einziger and Beyer, 2004), and (Spino et al, 1996)). For spent fuel pellets with burnups of 55 to 60 GWd/MTU, during reactor operation, about 8 percent of the noble gas atoms generated by the decay of fission products diffuse to particle grain boundaries and then escape to the rod free volume through the pellet's internal crack network ((Manzel and Walker, 2002) and (Einziger and Beyer, 2004)).

OUO-SRI
Ex 2
p. 44a

(U) In the rim layer, 0.1 to 0.3 μm subgrains are generated by the recrystallization of UO_2 and gas atoms in subgrain interiors migrate to subgrain boundaries, where they accumulate in micropores that were formed by clustering of lattice vacancies ((Manzel and Walker, 2002), Thomas et al, 1992), and (Spino et al, 1996)). Increase of gas pressure with time in these micropores is relieved by growth of micropore volumes (Manzel and Walker, 2002) (release of the energy stored in the pressurized gas in the micropore creates additional micropore surface by breaking U-O bonds at subgrain boundaries and by plastic deformation of subgrain boundary surface). Measurements ((Einziger and Beyer, 2004) and (Manzel and Walker, 2000)) show that the porosity of the rim layer ranges from about 10 to 20 percent with 15 percent being typical of fuel with burnups of 60 to 70 MWd/kgU ((Einziger and Beyer, 2004), (Manzel and Walker, 2000), and (Spino et al, 1996)).

(U) Because distances to grain boundaries are so short in rim layer subgrains, noble gas atoms formed by fission product decay migrate efficiently to rim layer subgrain boundaries.

Consequently, 90 percent of the noble gas atoms formed in the pellet rim layer are contained in the micropores that have formed on subgrain boundaries (Manzel and Walker, 2002).

Ex #2
p. 45a

(U) The volume of fuel pellets in a single BWR rod and the volume of the rim layer on these pellets are given by $V_{pellets} = \pi(d_{pellet}/2)^2 L_{active}$ and $V_{rim} = \pi d_{pellet} t_{rim} L_{active}$, and thus $V_{rim}/V_{pellets} = 4t_{rim}/d_{pellet} = 4(150\ \mu m/1.057\ cm) = 0.057$. But the capture of epithermal neutrons, that causes the rim layer to form, doubles the concentration of radionuclides in the rim layer compared to their concentration in the pellet body (Einziger and Beyer, 2004). Thus, about 11 percent of the total radionuclide inventory in the pellets in a rod resides in the friable rim layer of these pellets and the remaining 89 percent of the total inventory is contained in the body of the pellets. Accordingly,

$$F_{RC,k} = (0.11)(\text{rim release k}) + (0.89)(\text{body release k})$$

Ex2
OVD-SR4
p. 45b

OVD-SR4
Ex2
p. 45c

Ex #2
p. 45d

(U) The He fill pressure at 70 F of the rods in the 8x8 BWR assemblies is stated to range from 58.8 to 88.2 psig (TSAR[d]), which yields an average value of 5.0 atm = (58.8 psig+88.2 psig)/2(14.7 psig/atm). The TN-68 SAR states (Transnuclear, Inc., 2000) that the maximum initial He fill pressure of the rods in 8x8 BWR assemblies is 80 psig = 5.4 atm. Therefore, P_{He} = 5.0 atm at 70 F = 294 K and 10.5 atm at 349 C = 622 K, the temperature of 10 year cooled spent fuel (TSAR[c]).

(U) The ORIGEN calculation described above shows that one 8x8, 10-year cooled, high burnup BWR spent fuel assembly contains 90 g of Kr and 1436 g of Xe. Therefore, n_{total}, the number of moles of fission product noble gases in a single BWR rod, is

$$n_{total} = [(90\ g/83\ g\ mole^{-1}) + (1436\ g/131\ g\ mole^{-1})]/(64\ \text{rods per assembly}) = 0.188\ \text{moles}$$

(U) As noted above, about 10 percent of the fission product noble gas atoms in the body of a high burnup spent fuel pellet escape to the rod free volume during reactor operation or as a result of pellet fracturing.

ALL
OUO-SRI
EX2
p.46a

47a
OUO-SRI
Ex2

(U) Given these definitions

$$F_{rel,particles} = 0.11F_{imp,rim}\{[n_{tears/rod}F_{tear,rim}] + [F_{ent,rim}(F_{bed})]\} + 0.89\{n_{tears/rod}(F_{init,body} + F_{imp,body})(F_{bed})\}$$

(U) **Expressions for $F_{imp,body}$ and $F_{imp,rim}$.** The DOE Handbook (DOE, 1994) gives the following formula for F_{imp}, the fraction of a brittle material that is converted to respirable fines by impact fracturing:

$$F_{imp} = 2x10^{-11}\rho gh = 2x10^{-11}mgh/V = 2x10^{-11}(E/V) = 2x10^{-11}\rho(E/m)$$

where E/V and E/m are the energy per unit volume and per unit mass of the brittle material that is subject to fracturing and the units of the leading coefficient are $cm^3/ergs$.

(U) Figure 6-2 compares this equation [$F_{imp} = 2x10^{-11}\rho(E/m)$] to experimental data[2] for the impact fracturing of a variety of brittle materials including depleted and average burnup UO_2 pellets, but no high burnup spent fuel pellets. The figure shows that the handbook equation lies about a factor of 10 higher than the experimental data.

47b
OUO-SRI
Ex2

(U) The accumulation of noble gas atoms in the pores in the rim layer of high burnup spent fuel causes these pores to become highly pressurized, which means that substantial amounts of energy are stored in these pores. Because increase of gas pressure with time in rim layer pores is relieved by growth of pore volumes (Manzel and Walker, 2000), at any instant in time, the energy stored in pores will by itself be too small to initiate growth of grain boundary surfaces by breaking of U-O bonds or by plastic deformation of pore surfaces.

47c Ex2
OUO-SRI

[2] Personal communication, P. C. Reardon, January 2004.

Ex 2

OUO-SRI 48a Ex 2

Ex 1
p. 48b

Ex 2
OUO-SRI
p. 48c

Figure 6-2.

The contents of this figure are classified.

(U) The DOE Handbook equation was modified by letting

$$E = E_{Imp} + \alpha U_{Pores}$$

48d
OUO-SRI
Ex 2

SGI

499
EX 2
OUO-SRI

(U) Pore pressure can be calculated using the ideal gas law by setting V equal to the rim layer volume times the porosity of the rim layer and letting n equal the number of moles of fission product noble gases in the rim layer. Thus,

$$P_{pore} = n_{rim} \frac{RT}{F_{pores,rim} V_{rim}}$$

OUO-SRI EX 2
p. 49 b

(U) Spino et al. (Spino et al, 1996) state that a high burnup rim that has a local burnup of 70 Gwd/tM also has a concentration of about 0.0106 g Xe per g UO_2, a matrix density of 10.72 g/cm^3, a porosity of 15 percent, a mean pore diameter of 1.4 μm, about 7.09×10^{-15} moles of Xe per pore, and two and three dimensional pore densities of 0.1 pore/μm^2 and 9.12×10^7 pores/mm^3. Therefore,

$$\frac{n_{Xe\,rim}}{V_{rim}} = \left(\frac{0.0106\,g\,Xe}{g\,UO_2}\right)\left(\frac{10.72\,g\,UO_2}{cm^3}\right)\left(\frac{1\,mole\,Xe}{131\,g\,Xe}\right) = 8.7 \times 10^{-4}\ \text{moles Xe cm}^{-3}$$

$$n_{Xe/pore} = \frac{8.7 \times 10^{-4}\ \text{moles Xe cm}^{-3}}{9.12 \times 10^{10}\ \text{pores cm}^{-3}} = 9.5 \times 10^{-15}\ \text{moles Xe pore}^{-1}$$

which agrees well with the value of 7.09×10^{-15} moles Xe pore^{-1}, and

$$V_{pore} = \frac{4}{3}\pi\left(\frac{d_{pore}}{2}\right)^3 = \frac{4}{3}\pi\left(\frac{1.4\,\mu m}{2}\right)^3\left(1\,cm^3/10^{12}\,\mu m^3\right) = 1.4 \times 10^{-12}\ cm^3$$

(U) This data allows P_{pore} to be calculated in two ways. First,

$$P_{pore} = \frac{1}{F_{pores}} \frac{n_{rim}}{V_{rim}} RT$$

OUO-SRI
P50a
Ex2

and second,

OUO-SRI
P50b
Ex2

OUO-SRI
Ex2
P50c

(U) Since the noble gas filled pores in the rim are located on subgrain boundaries, an alternative value for the number of pores per mm^3 in the rim layer can be estimated as the product of the two dimensional pore density and the subgrain surface area per mm^3 of rim material. Since the rim subgrains are cubes with an average side length of 0.2 μm, the volume of a subgrain is 0.008 $\mu m^3 = 8x10^{-12}$ mm^3, the number of subgrains per mm^3 of rim layer is $1/(8x10^{-12}$ $mm^3) = 1.25x10^{11}$, and $A_{subgrains}$, the subgrain surface area per mm^3, is the number of subgrains per mm^3 times the surface area of one subgrain divided by two since each subgrain face is shared by another subgrain. Thus, $A_{subgrains} = [1.25x10^{11}$ subgrains/$mm^3][6(0.2$ $\mu m)^2]/2 = 1.5x10^{10}$ $\mu m^2/mm^3$, and the number of pores per mm^3 is the number of pores per μm^2 times the subgrain surface area per $mm^3 = (0.1$ pores/$\mu m^2)(1.5x10^{10}$ $\mu m^2/mm^3) = 1.5x10^9$ pores/mm^3, which is about a factor of 15 larger than the value of $9.12x10^7$ pores per mm^3 developed by Spino et al. (Spino et al, 1996). So if this pore density were used to calculate the pore energy per cm^3, a value of $U_{pores} = 15(4.2$ J/$cm^3) = 63$ J/cm^3 would be obtained. Since the two estimates of the pore energy per cm^3 differ substantially, to be conservative, the average of the two values, 34 J/cm^3, is used to calculate $E_{Imp,rim}$.

(U) **Estimation of α.**

P50d
OUO-SRI
Ex2

Ex 2
P. 5/a
OUO-SRI

where the two in the denominator of the expression for $S_{subgrains}$ corrects for the fact that each subgrain face is shared by two subgrains. Therefore,

P51b
OUO-SRI
Ex 2

[redacted]

aw-sm
ex#2
p 52a

[redacted]

P52b
aw-sm
Ex 2

OUO-SRI
Ex 2
p. 53a

OUO-SR
Ex 2
p. 54

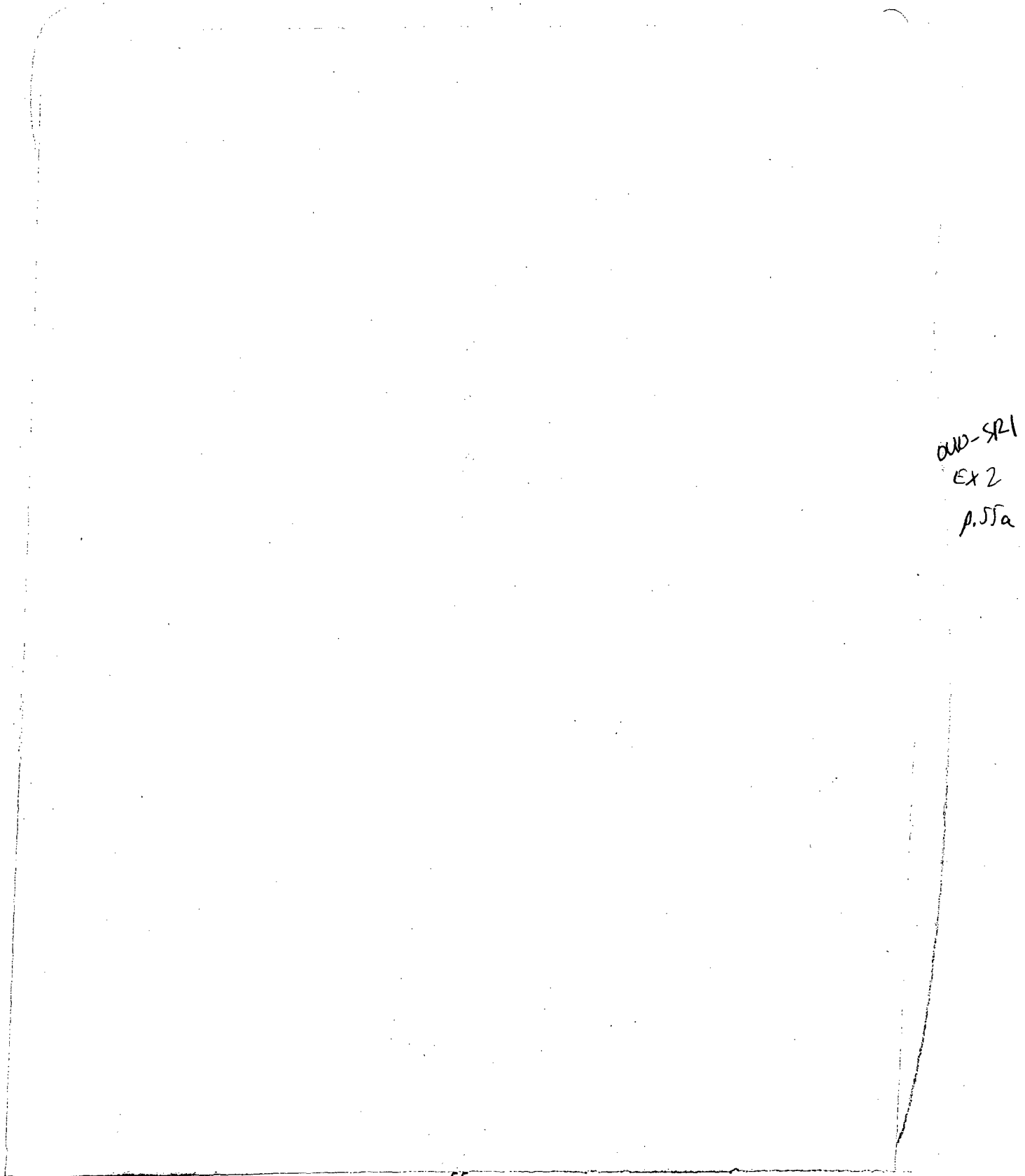

OWD-SR1
Ex 2
p. 55a

56a
Ex 2
OUO-SRI

56b
SG 1
Ex 3

$P_{rod\ failure}$ = the pressure that the canister would reach upon rod failure if blowdown of the canister to the environment were not occurring, and

F_{exp} = the fraction of the gases in the canister atmosphere that is released to the environment by canister depressurization.

(U) $P_{rod\ failure}$ is calculated using the ideal gas law. Let

P_{rod} = the pressure of He and fission product noble gases in a rod at ambient conditions

V_{rod} = the free volume of a spent fuel rod

n_{rod} = the number of moles of He plus fission product noble gases in a 10-year cooled high burnup spent fuel rod

$P_{canister}$ = the pressure of He fill gas in the HI-STORM canister at ambient conditions

$V_{canister}$ = the free volume of the HI-STORM canister

$n_{canister}$ = the number of moles of He fill gas in the HI-STORM canister

R = the ideal gas law constant

T = the average temperature of the canister interior and the spent fuel rods in the canister at ambient conditions

$P_{final} = P_{rod\ failure}$

N_{rods} = the number of spent fuel rods in the canister

V_{final} = the sum of the canister free volume plus the total free volume of the failed rods

(U) Given these definitions

$$P_{rod}V_{rod} = n_{rod}RT$$
$$P_{canister}V_{canister} = n_{canister}RT$$
$$P_{final}V_{final} = n_{final}RT$$
$$n_{final} = F_{rods}N_{rods}n_{rod} + n_{canister}$$
$$V_{final} = F_{rods}N_{rods}V_{rod} + V_{canister}$$

and substitution yields

$$P_{rod\ failure} = P_{final} = \frac{F_{rods}N_{rods}P_{rod}V_{rod} + P_{canister}V_{canister}}{F_{rods}N_{rods}V_{rod} + V_{canister}}$$

(U)

P57a
Ex 2
OUO-SRI

(U) For the HI-STORM canister $V_{canister}$ = 6.0 m^3 (TSAR[g]) and N_{rods} = (68 assemblies per cask)(64 rods per assembly) = 4352. For 10 year cooled spent fuel T_{rod} = 660 F = 349 C = 622 K (TSAR[c]) and, as derived above, F_{rods} = 1.0, V_{rod} = 41 cm^3 and P_{rod} = 40 atm.

P57b
Ex 2
OUO-SRI

SGI
EX 3
p 58

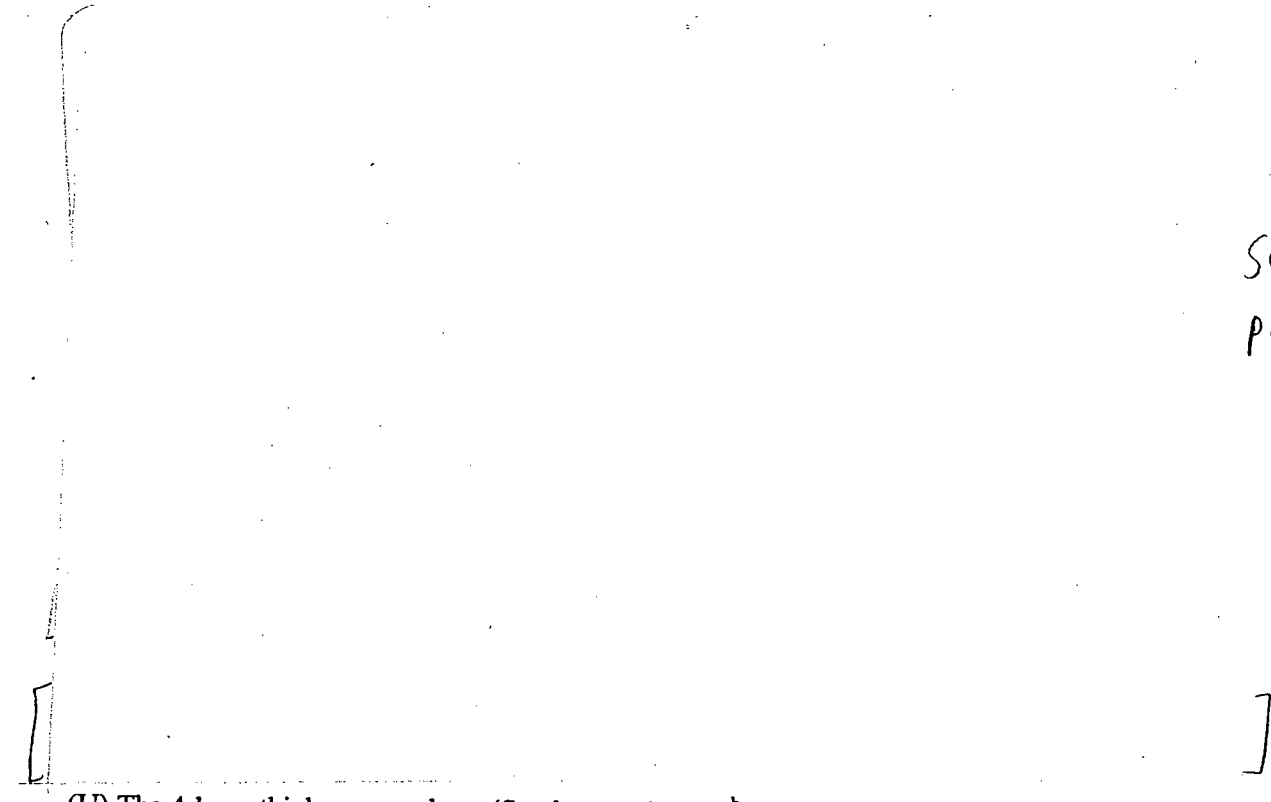

EX 3
SGI
p. 59a

Ex. 2
p. 59b

(U) The 4.1 cm thick spacer plates (Sanders et al, 1990[b]) in a 14 cm square (Sanders et al, 1990[c]) 8x8 BWR spent fuel assembly are fabricated as an 8x8 matrix of short 1.75 cm square tubes.

Ex. 2
p. 59c

Ex. 2
p. 59d

Ex. 2
p. 59e

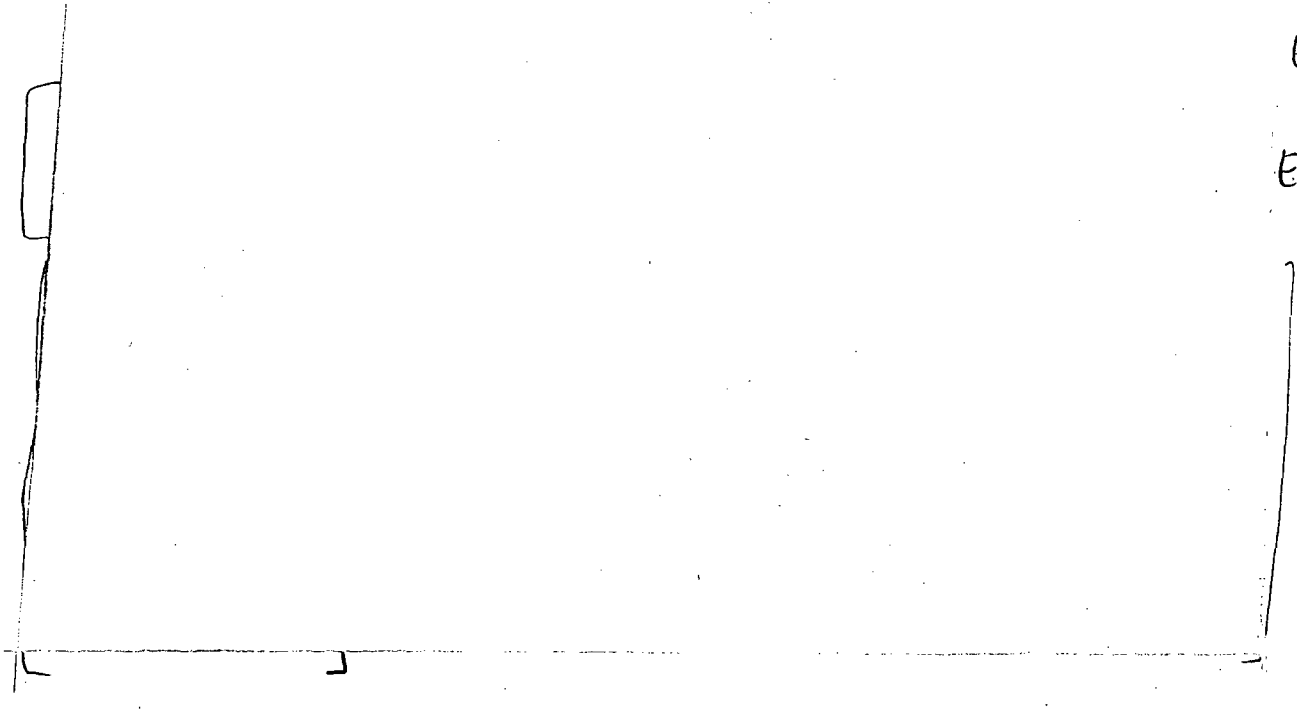

SGI
EX 3
p. 59f

(U) Measurement of the hydraulic diameters of sections of average and high burnup spent fuel rods show that average and high burnup spent fuel rod sections respectively have hydraulic diameters of about 50 and 35 μm (Vankeerberghen, 1995). The greater swelling of high burnup spent fuel pellets compared to average burnup spent fuel pellets causes the cracks in the internal crack network in high burnup pellets to have smaller crack widths. Accordingly, because the porosity of the rim layer in high burnup pellets is not significantly interconnected, even though the rim layer porosity is about 15 percent, while the porosity of the pellet body is typically about 3 to 6 percent [24-26,28], gas flow through the rim layer is not significant.

EX 3
SGI
p. 60a

SGI
EX 3
p. 60b

SGI
EX 3
1.60c

SGI
EX 3
1.60d

SGI
EX 3
p.60e

Ex 3
SGI
p. 61a

Ex 3
SGI
p. 61b

ex 2
p. 61c

ex 2
p. 61d

ex 2
p. 61e

ex 2
p. 61f

SGI
Ex 3
p. 61g

[

SGI
EX 3
p. 62 a

EX 3
SGI
p. 62
b

EX
1
p. 62
c

Classified

[

EX
3
SGI
p. 62 d

[3] Personal communication, R. L. Sullivan, U. S. Nuclear Regulatory Commission, October 2003.

SGI EX 3 p. 63a

SGI EX 3 63b p

EX 1 p. 63c

SGI EX 3 p. 63d

Classified

~~CONFIDENTIAL~~

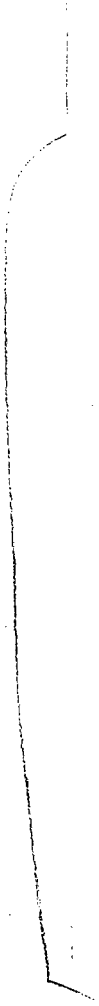

EX 3
SGI
p. 64a

Ex 3
SGI
p. 65a

Ex 3
SGI
p. 65b

Ex 3
SGI
p. 65c

Ex. 2
p. 65d

Classified
EX 1
p. 65e

~~CONFIDENTIAL~~

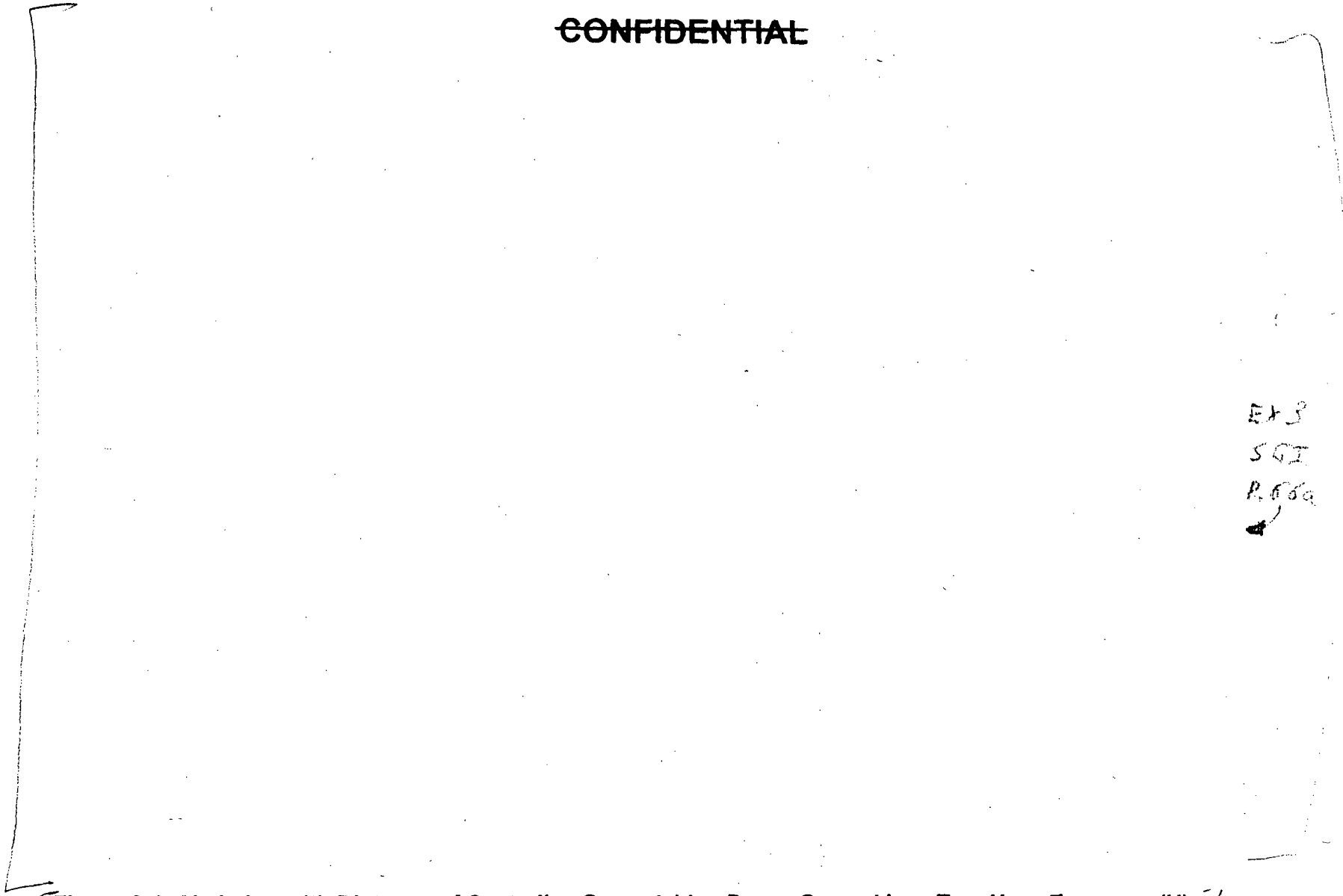

Figure 6-4. Variation with Distance of Centerline Groundshine Doses Caused by a Two-Hour Exposure (U)
The contents of this figure are unclassified.

SGT
Ex 3
p. 67a

~~CONFIDENTIAL~~

EX 3
SGI
p. 68

SGI
EX 3
p. 69a

SGI
EX 3
p. 69b

(U) The length and width of a typical BWR assembly are respectively 3.8 and 0.15 meters (DOE, 1995).

EX 3
69c

EX 3
SGI 69d

(U)[

Ex 3
SGI
p.70a

Ex 3
p.70b

SGI
Ex 3
p. 70c

SGI Ex 3
p.70d

SGI
EX3
p.70e

Claims
Ex 1
p.70f

Claim Aid
Ex 1
p.70g

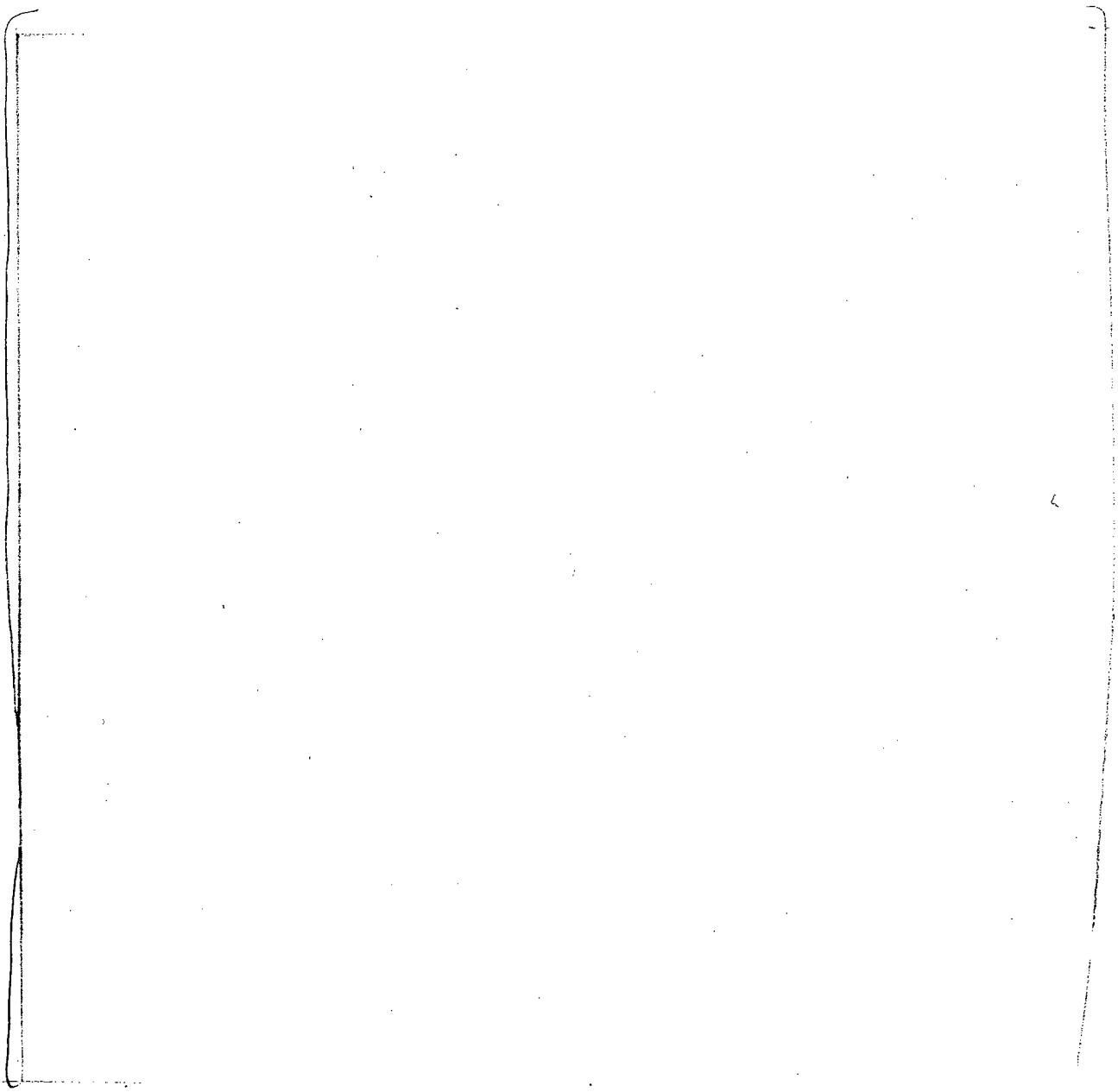

Ex. # 2
p. 71a

7 Summary (U)

(U) A large design basis threat (DBT) explosive charge blast attack on a HI-STORM dry spent nuclear fuel cask was evaluated.

SGI
p. 72a
Ex3

(U) The source term calculations result in the largest uncertainty affecting the consequence calculations.

SGI
72b
Ex3

8 References (U)

(U) Beal, S.K. 1978. "Correlations for the Sticking Probability and Erosion of Particles," J. Aerosol Sci., 9, 455.

OUO-SRI Ex 2 73a

(U) Chung, J., Ed. (2003). *Health and Safety Manual*, Chap. 7, App. E, "Stored Energy of a Pressurized Gas Vessel", LBNL/PUB-3000, Lawrence Berkeley National Laboratory, Berkeley CA, available at http://www.lbl.gov/ehs/pub3000/.

(U) Code of Federal Regulations (CFR). Volume 49, Part 173.435 (49 CFR 173.435).

(U) Croff, A.G. 1980. *ORIGEN2 - A Revised and Updated Version of the Oak Ridge Isotope Generation and Depletion Code*, ORNL-5621, Oak Ridge National Laboratory, Oak Ridge, TN.

a) Ref. 7, Section 7.2.2, Accident Source Terms, p. 7-13.
b) Section 5.4.1, Rod Failure Strain Criterion, p 5-28.
c) Section 7.3.3, Particles, p 7-30.
d) Section 7.3.6, CRUD, p. 7-48.
e) p.7-21.
f) Section 8.12 Loss of Shielding Accidents, p. 8-47.

OUO-SRI Ex 2 73b

(U) DOE (1995). Integrated Data Base Report, DOE/RW-0006, Rev.12, U. S. Department of Energy Office of Environmental Management, Table 1.4.

(U) Dobratz, B. M. and P. C. Crawford (1985). "LLNL Explosives Handbook. Properties of Chemical Explosives and Explosive Simulants," Lawrence Livermore National Laboratory Report, UCRL- 52997, Change 2, January 1985.

(U) Einziger, R.E. and C. Beyer. (2004). *Characteristics of High Burnup Fuel that May Affect the Transportation Source Term*, white paper prepared for the NRC spent fuel package vulnerability study, copy available on request from Jeremy Sprung, (505) 844-0134.

(U) Environmental Protection Agency (EPA). 2001. *Air Quality Criteria for Particulate Matter, Volume I*, EPA 600/P-99/002aB, Office of Research and development, Washington DC 20460, p. 2-38.

(U) Fromentin, A. (1989). *Particle Resuspension from a Multilayer Deposit by Turbulent Flow*, PSI-Bericht Nr. 38, Programm LWR-Sicherheit, Paul Scherrer Institute.

(U) Geelhood, K and C. Beyer. (2003). *Examination of Strain to Failure Data from Irradiated Zircaloy*, white paper prepared for the NRC spent fuel package vulnerability study, copy available on request from Jeremy -, (505) 844-0134.

(U) Golubev, I.F. (1970). *Viscosity of Gases and Gas Mixtures, A Handbook*, Israel Program for Scientific Translations, Jerusalem, Table 4, p. 62.

(U) Group GMX-6 (1969). "Selected Hugoniots," Los Alamos Scientific Laboratory Report LA-4167-MS.

(U) Hazelton, R. F. (1987). Characteristics of Fuel Crud and Its Impact on Storage, Handling, and Shipment of Spent Fuel, PNL-6273, Pacific Northwest Laboratory, Richland WA 99352, September 1987.

(U) Hertel, E. S., R. L. Bell, M. G. Elrick, A. V. Farnsworth, G. I. Kerley, J. M. McGlaun, S. V. Petney, S. A. Silling, P. A. Taylor, and L. Yarrington (1993). "CTH: A Software Family for Multi-Dimensional Shock Physics Analysis," SAND92-2089C, Sandia National Laboratories, Albuquerque, NM, July 1993.

(U) Hertel, E. S., and G. I. Kerley (1998). "CTH Reference Manual: The Equation of State Package," SAND98-0947, Sandia National Laboratories, Albuquerque, NM, April 1998.

(U) HOLTEC International. 2000. *HI-STORM Topical Safety Analysis Report*, Revision 10, Holtec International Report No. HI-951312, Holtec International, Marlton, NJ (available from NRC document room).

(U) International Atomic Energy Agency (IAEA) (1987). Safety Series No. 7, IAEA Safety Guides, Explanatory Material for the IAEA Regulations for the Safe Transport of Radioactive Material (1985 Edition), 2nd Edition, Vienna.

(U) Iversen, J. D. (1984). *Particulate Entrainment by Wind*, Project 1699, ISU-ERI-Ames-85010, Department of Aerospace Engineering, Iowa State University, Ames Iowa, Report prepared for Los Alamos Scientific Laboratory.

(U) Johnson, G. R. and T. J. Holmquist (1989). "Test Data and Computational Strength and Fracture Model Constants for 23 Materials Subjected to Large Strains, High Strain Rates and High Temperatures," Los Alamos National Laboratory Report LA-11463-MS (Limited Access).

(U) Kass, W. J. (1985). "MC2893A and MC3599 Heat Source Development," Sandia National Laboratories Report SAND84-1625, March 1985.

(U) Kipp, M. E. (2003). Personal Data.

(U) Kipp, M. E. (2004). "Response of Two Nuclear Fuel Transportation Casks to Large Explosive TNT Charges," Sandia National Laboratories Report, SAND2004-xxxx, January, 2004. (CNSI).

(U) Lorenz, R. A. et al. (1980). *Fission Product Release from Highly Irradiated LWR Fuel*, NUREG/CR-0722, Oak Ridge National Laboratory, Oak Ridge TN, pps 48-80.

(U) Lukic, J. D., and Schmidt, J. S. (2003). Taming the CRUD Proglem: A Utility Perspective, Nucl. Technol. **142**, 283.

(U)

Ex 2
p. 75a

(U) Manzel, R. and Walker, C.T. (2000). High Burnup Fuel Microstructure and its Effect on Fuel Rod Performance, Proc. Intl. Topical Meeting on LWR Fuel Performance, Park City Utah, April 2000.

(U) Manzel, R. and Walker, C. T. (2002). EPMA and SEM of fuel Samples from PWR Rods with an Average Burn-up of Around 100 MWd/kgHM, Journal of Nuclear Materials, **301**, 170.

(U) Marsh, S. P. (1980). "LASL Shock Hugoniot Data," University of California Press, Berkeley.

(U) McGlaun, J. M., S. L. Thompson, and M. G. Elrick (1990). "CTH: A Three-Dimensional Shock Wave Physics Code," Int. J. Impact Engng., 10, 351-360.

(U) Oak Ridge National Laboratory (ORNL) (1991). ORIGEN2 Isotope Generation and Depletion Code, CCC-371, Oak Ridge National Laboratory, Oak Ridge, TN.

(U) Otani, Y. (1989). *Aerosol Science Technol.* 10, 463 (1989).

(U) Ranz, W. E. (1958). *Principles of Inertial Impaction*, Bulletin No. 66, Department of Engineering. Research, Pennsylvania State University, University Park, PA, Fig. 8, P. 21.

(U) Sanders, T.L., Seager, K.D., Rashid, Y.R., Barrett, P.R, Malinauskas, A.P., Winziger, R.E., Jordan, H., Tomas, A.D., Sutherland, S.H., and Reardon, P.C. (1992). *A Method for Determining the Spent-Fuel Contribution to Transport Cask Containment Requirements*, SAND90-2406, Sandia National Laboratories, Albuquerque, NM:

a) Figure III-60, p. III-107
b) Table I-3, p. I-11.
c) Table I-5, p. I-19.
d) Table I-4, p. I-16.

e) Figure IV-1, p. IV-12.

(U) Sandoval, R. P., *et al.* (1983). "An assessment of the Safety of Spent Fuel Transportation in Urban Environs," Sandia National Laboratories Report SAND82.2365.

(U) Sandoval, R. P. et al. (1991). *Estimate of CRUD Contribution to Shipping Cask Containment Requirements*, SAND88-1358, Sandia National Laboratories, Albuquerque, NM :

a) p. 13.
b) Figure I-13, p. I-40.

Ex # 2
p. 76a

[redacted]

(U) Shleien, B. et al. (1998). *Handbook of Health Physics and Radiological Health*, Williams & Wilkins, Table 6.2.2.

(U) Spino, J., K. Vennix, and M. Coquerelle. (1996)." Detailed Characterization of the Rim Microstructure in PWR Fuels in the Burn-up Range 40-67 GWd/tM," *Journal of Nuclear Materials*, 231, 179 (1996).

(U) Sprung, J. L. et al. (1998). *Data and Methods for the Assessment of the Risks Associated with the Maritime Transport of Radioactive Materials: Results of the SeaRAM Program, Vol. 2, Appendix IV, Cask-to-Environment Release Fractions*, SAND98-1171, Sandia National Laboratories, Albuquerque, NM:

a) Figure 6-1, p. 6-6.

(U) Sprung, J.L. et al. (1990). *Evaluation of Severe Accident Risks: Quantification of Major Input Parameters*, NUREG/CR-4551, U.S. Nuclear Regulatory Commission, Washington DC 20555.

(U) Sprung, J. L., D.J. Ammerman, N.L. Breivik, R.J. Dukart, F.L. Kanipe, J.A. Koski, G.S. Mills, K.S. Neuhauser, H.D. Radloff, R.F. Weiner, H.R. Yoshimura. (2000). *Reexamination of Spent Fuel Shipment Risk Estimates*, NUREG/CR-6672, U.S. Nuclear Regulatory Commission, Washington, DC (available at ttd.sandia.gov/nrc/modal.htm), Section 7.3.4, Cesium, p. 7-35.

(U) Steinberg, D. J. (1996). "Equation of State and Strength Properties of Selected Materials," Lawrence Livermore National Laboratories Report UCRL-MA-106439, Change 1, February 1996.

(U) Thomas, L. E. C. E. Beyer, and L. A. Charlot. (1992). "Microstructural Analysis of LWR Spent Fuel at High Burnup," *Journal of Nuclear Materials*, 188, 80 (1992).

(U) Topical Safety Analysis Report (TSAR) (Rev. 10) with Certificate of Compliance No., 1014 for the HI-STORM 100 Cask System, Holtec Report HI-951312

a) Table 2.0.1, p. 2.0-17
b) Table 2.0.2, p. 2.0-26.
c) Table 2.2.3, p. 2.2-23.
d) Table 4.3.5, p. 4.3-14.
e) Table 2.1.4, p. 2.1-14.
f) Table 4.4.14.
g) Table 4.4.13.
h) Drawing 1401 Sheet 2.

(U) Transnuclear, Inc. (2000). *TN-68 Dry Storage Cask Final Safety Analysis Report*, Revision 0, Transnuclear, Inc., Hawthorne, NY (available from NRC document room):

a) Table 5.2-1.
b) Table 5.2-2.
c) Table 5.2-1.

(U) Vankeerberghen, M. (1995). *Recent Gas Flow Measurements in IFA-504 Rods*, HWR-433, Halden Reactor Project, Halden, Norway.

(U) Weast, R. C., Ed. (1966). *Handbook of Chem. and Phys., 47th Edition*, R. C. Weast, Ed., The Chemical Rubber Co., Cleveland OH 44114, 1966,

a) p. F-40.
b) Table 4-1, p. 4-3 and Figures 4-1a and 4-1b, p. 4-5.

[redacted]

Ex #2
p. 77a

Appendix A: Catalogue of Material Model Parameters (U)

(U) Parameters for the material models used to represent the HI-STORM cask, fuel basket assembly, and explosive are catalogued in this appendix. The nomenclature in the tables generally follows the keyword inputs for CTH. CTH model input parameters are in units of cm-g-sec-eV (298 K = 0.0256798 eV).

(U)[

Ex 2
PAI-a

The model parameters define the release isentrope of the product gases through the Chapman-Jouguet steady detonation state (Table A-1).

Table A-1: Material Parameters for TNT Explosive (U)
The contents of this table are unclassified

Parameter	TNT
Density, ρ g/cm^3 (lb/ft^3)	1.63 (101.1)
Detonation Velocity cm/s (in/s)	6.93×10^5 (2.73×10^5)
C-J Pressure GPa (psi$\times10^6$)	21.0 (3.0)
Ideal Gas Constant, Γ	2.727
A dynes/cm^2 (psi)	3.712×10^{12} (5.38×10^{10})
B dynes/cm^2 (psi)	3.231×10^{10} (4.685×10^8)
C dynes/cm^2 (psi)	1.045×10^{10}(1.515×10^8)
R_1	4.15
R_2	0.95
ω	0.30
C-J Temperature (eV)	0.35

(U) CTH decouples material behavior into dilatational and deviatoric response, where the dilatational response is described by an equation of state (EOS), and the deviatoric response is described by a yield strength model (*i.e.*, an elastic-plastic model). The equation of state EOS expresses a relationship between the thermodynamic pressure, density, and internal energy in a state of equilibrium. The basic solid equation of state for the inert materials is Mie-Gruneisen, in which the reference state is the Hugoniot, here defined by a linear shock velocity – particle velocity relationship. This equation of state defines the pressure response in the material with separate volumetric and thermal terms, where the thermal contribution is a linear function of the internal energy. The solid Hugoniots were drawn from data found in Group GMX-6 (1969) and Marsh (1980) data summaries. Air was treated with a pre-defined tabular equation of state, SESAME 5030 (Hertel and Kerley, 1998). Yield strength parameters were drawn from a variety

of sources, including Steinberg (1996) and Johnson and Holmquist (1989), which includes strain-hardening effects for the stainless steel. The fracture (spall) stress for each material has also been included in these tables; fracture occurs at this minimum stress, effected by inserting void into a cell to relax the tensile stress to zero.

(U) The parameters for the HI-STORM storage container are listed in Table A-2. Concrete was represented as a porous solid, with pressure-dependent yield strength. The parameters were drawn from a 5 ksi concrete model that has been tested against WES penetration experiments (Kipp, 2003). The uniaxial strain response compared to data from triaxial tests is shown in Figure A-1.

ε_x # 2
p. A-2a

ε_x # 2
p. A-2b

Note: 1 kg/m^3=0.062 lb.ft^3; 1 m/s=3.28 ft/s; 1 J/kg-K=2.39e-4 Btu/lb-°F; °F=1.8*T_k - 459.67; 1 MPa=145 psi

(U) The spent fuel tube contents are modeled as a homogeneous porous material, represented by a P-α model (Table A-3). The state variable α relates the porous material density to the density of the fully dense material, in this case the UO_2. This model permits the fuel within the tube to undergo some crushing under small loads until the void has been fully removed, after which the material responds as the stiff, fully dense ceramic. The reference density of 5100 kg/m^3 is estimated from the mass of the fuel rods and other materials inside the tube, accounting for the total volume available.

Table A-3. CTH material parameters for 24 Element MPC-24 Fuel Basket Assembly.
The contents of this table are unclassified.

ex. 2
p. A-3a

[Note: 1 kg/m^3=0.062 lb.ft^3; 1 m/s=3.28 ft/s; 1 J/kg-K=2.39e-4 Btu/lb-°F; °F=1.8*T_k - 459.67; 1 MPa=145 psi]

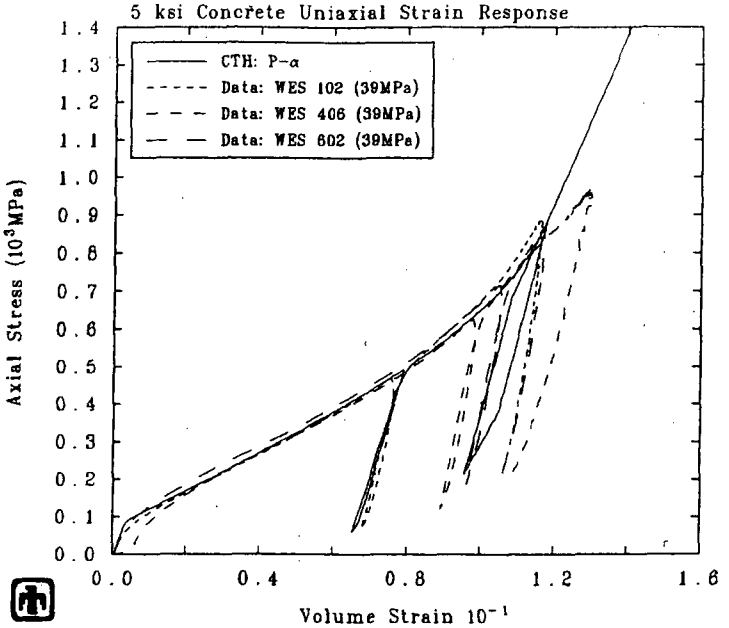

Figure A-1. Uniaxial strain load – unload response for a 34.5 MPa (5 ksi) concrete (1 MPa = 145 psi) (U).

The contents of this figure are unclassified.

Appendix B: Container Wall "Fluffing" to Accommodate Resolution (U)

(U) Both the container wall of the HI-STORM storage cask and the canister wall are relatively thin compared to the resolution accessible in the CTH simulations. In order to accommodate this disparity, minimize artificial wall erosion, and provide sufficient confinement during the passage of the detonation products and blast wave, two walls were modified by increasing their thickness, while preserving the mass and circumferential strength of the wall. This "fluffing" technique then allows these walls to be resolved by at least a few cells, and thereby retain some measure of integrity.

P.B-1a EX2 OUO-SR1

These modifications are apparent in transverse cross-sections shown in Figure B-1. For the exterior shell, the outer radius was preserved and the interface between the steel and the concrete relocated inwards. In order to approximately preserve the mass of the original steel shell and displaced concrete, the thickened shell material was changed to aluminum, and the yield strength reduced to 70 MPa (10.2 ksi) to provide a confinement strength comparable to that of the original steel shell. The inner wall radius of the MPC stainless canister was already at a minimum with respect to the fuel assemblies, so the exterior radius was increased, utilizing the free space normally occupied by a set of vertical thin-walled U-shaped elements that centered the MPC in the storage container and provided air circulation.

P.B-1b EX2 OUO-SR1

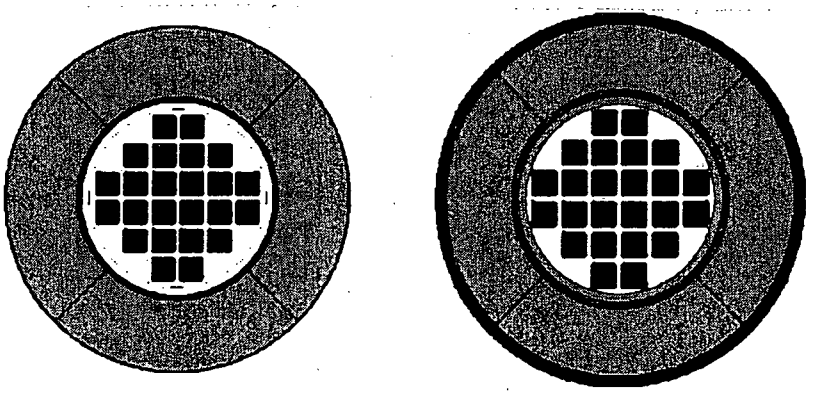

Figure B-1. Reference condition of storage container model with original outer steel wall thickness and canister aluminum shell (left) compared with "fluffed" outer steel and canister aluminum walls (right) ($\Delta x = 2.5$ cm (1.0 in)). (Section through mid-plane of explosive charge.) (U)

The contents of this figure are unclassified.

(U) The difference made by the thickness expansion in the shell integrity characterized by the code (CTH) can be readily seen in Figures B-2 (external view of the storage container) and B-3 (view of the MPC canister). The mottled surface of the storage container in Figure B-2 (left) indicates that with the original thickness, the steel and concrete are all mixed material cells, and no specific shell exists as an explicit layer; the fluffed layer clearly indicates a substantial shell is present (right image in Figure B-2). A similar situation exists for the MPC canister wall, where the original thickness is not discernable as a shell at all (left image in Figure B-3), whereas the fluffed shell is well defined (Figure B-3, right).

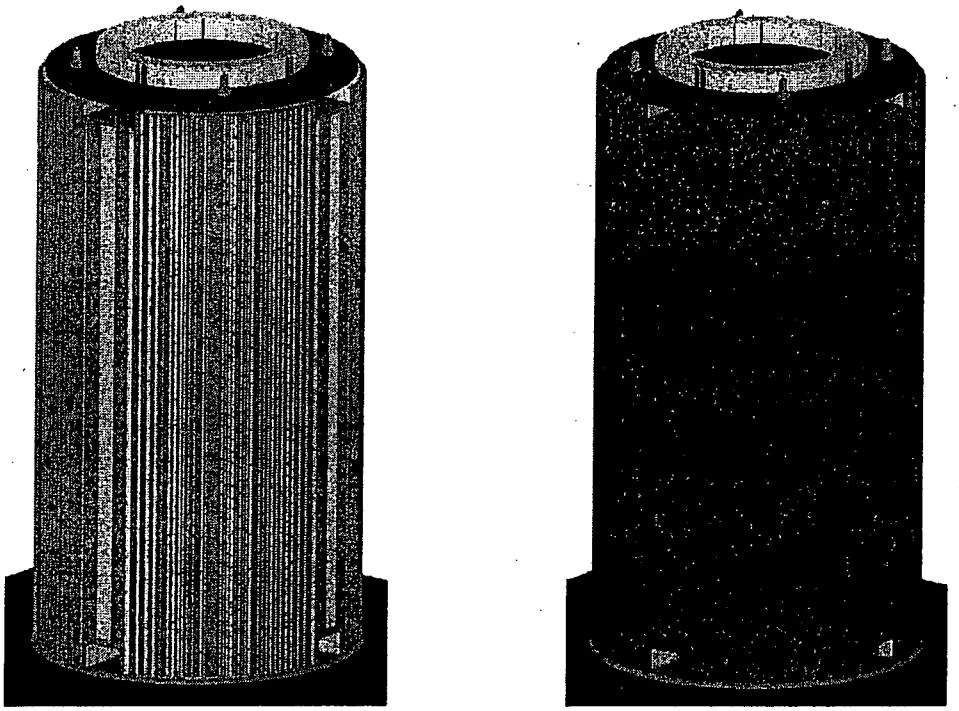

Figure B-2. Perspective view of reference condition of storage container model with original outer steel wall thickness and canister aluminum shell (left) compared with "fluffed" outer steel and canister aluminum walls (right) (Δx = 2.5 cm (1.0 in)) (U).

The contents of this figure are unclassified.

PB-2a SG1 Ex3

External views of the storage containers (Figure B-4) indicate that there is not a significant superficial difference in the shape and volume of the crater formed in the container directly under the explosive charge. The thickened shell, however, makes it considerable more clear how the metal has been moved as a result of the large deformation associated with the blast incident on the container. The cross-sections in Figure B-5, however, indicate that the lack of integrity of the two original shells leads to considerable more

expansion of the MPC canister (left) than when the shells have a thickness that can be resolved by a few computational cells (right).

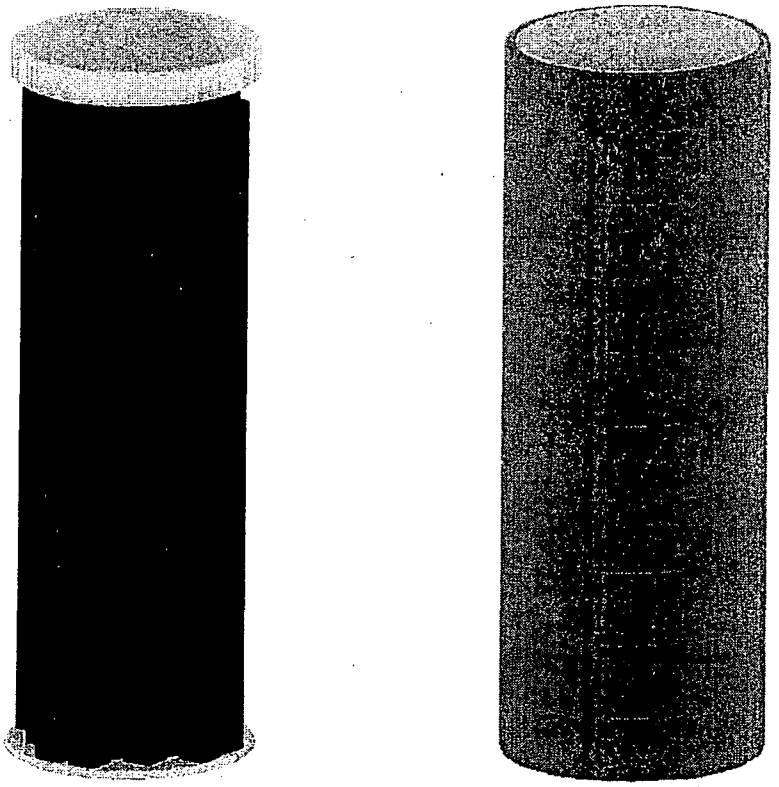

Figure B-3. Perspective view of reference condition of canister model with original outer steel shell (left) compared with "fluffed" outer canister shell (right) (Δx = 2.5 cm) (U).
The contents of this figure are unclassified.

(U) The overall deformation seen in a vertical section (Figure B-6) is also not too much altered by the thickness increase of the two shells. The primary improvement afforded by the shell fluffing is recorded in the images of the MPC canister in Figure B-7. With the original thickness, it is not possible to glean any information from the deformed shell regarding its final integrity in protecting the contents from release (left).

P.B-3a
SG1
Ex 3

ex. 2
p. B-4a

ex. 2
p. B-4b

Ex. 2
p. B-5a

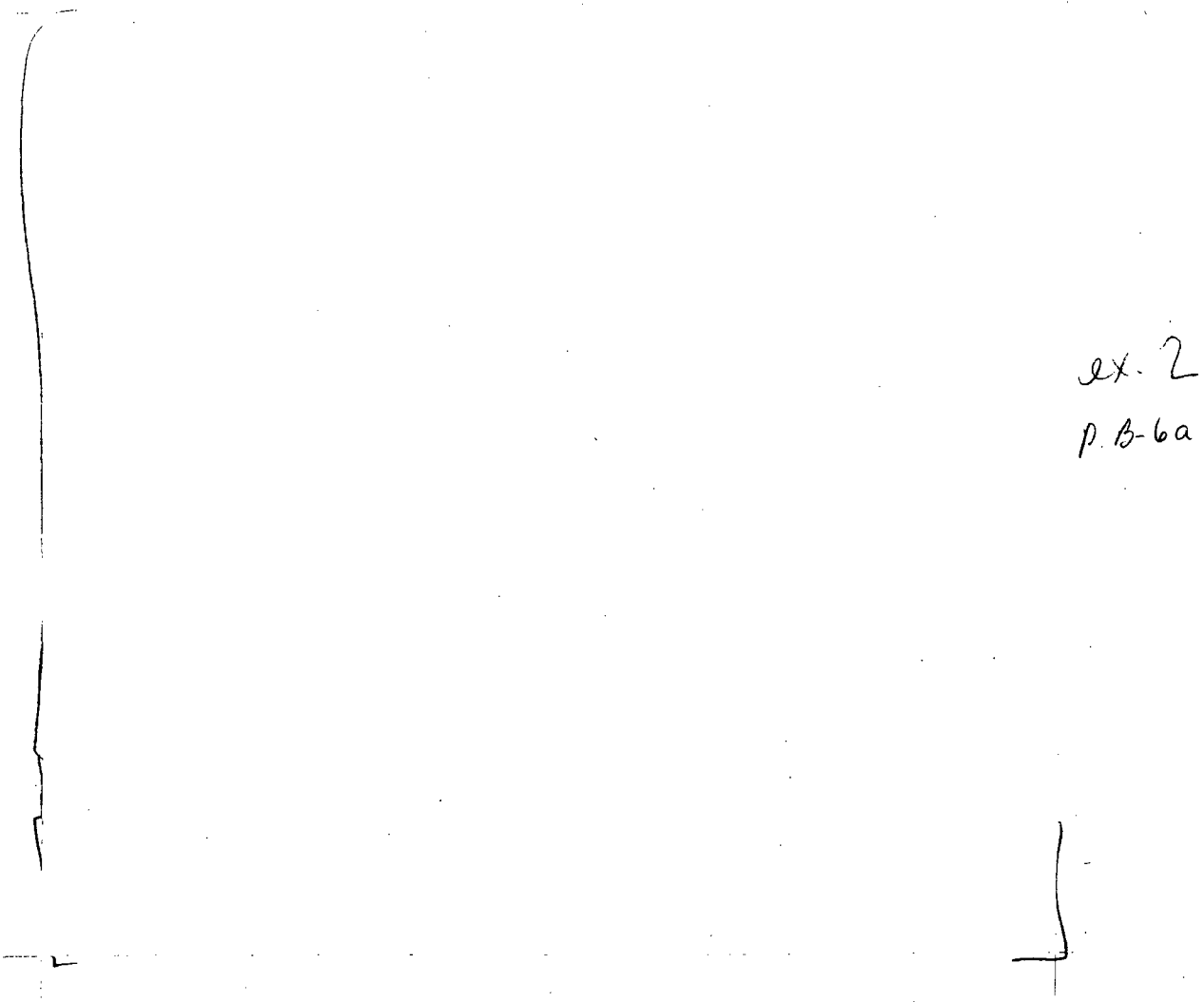

ex. 2
p. B-6a

Appendix C: Fuel Internal Energy States – Homogeneous and Explicit Models (U)

(U) As noted in Section II of this document, each of the 24 individual fuel assemblies in the three-dimensional simulations was modeled as a homogeneous material with an effective density of the fuel plus the porosity (void) in the assembly. This porous material model allows the crushing out of the void until the density of the UO_2 is recovered (10.3 g/cm^3), after which the material response follows that of the fully dense material. In order to estimate the potential for the formation of respirable UO_2 aerosols from these assemblies, an energy-based criterion is used: the mass fraction of aerosols formed has been correlated to the internal energy density state of the fuel (Luna, *et al.*, 1999; Sandoval, *et al.*, 1983).

(U) The use of the energy criterion is complicated, though, by observations that when subjected to identical shock loads, the internal energy density increase in the distributed fuel is not identical to that of the UO_2 in an explicitly modeled fuel pellet. That is, a conversion factor is needed to apply to the energy density values obtained from the HI-STORM simulation to relate them to an appropriate energy density for the pellets in explicit fuel assemblies[

ex# 2
p. C-1a

C.1 Single-Pellet Impact (Clad) (U)

(U)[

Ex# 2
p. C-1b

For the homogeneous fuel case, the identical impact condition was maintained, and the mass of the fuel set to the sum of the UO_2 and zircalloy cladding. The right hand boundary condition was set to zero displacement, to simulate the fuel situated on a rigid anvil.

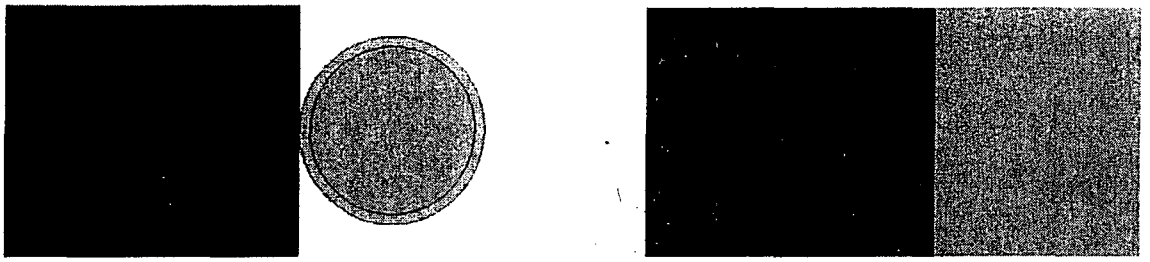

Figure C-1. Single clad fuel pellet impacted by a steel slug (left). The corresponding steel slug / homogeneous fuel is shown on the right (U).

The contents of this figure are unclassified.

(U) The sequence of images in Figure C-2 illustrates the impact and crushing of the fuel in both the explicit pellet (left) and homogeneous fuel (right) configurations. The total internal energy of the fuel, normalized by the fuel mass to obtain an average energy density for the fuel, is plotted for both cases in Figure C-3. These energy density histories indicate that the homogenous configuration leads to an energy density about a factor of 1.6 larger than the explicit pellet model fuel sustains.

(U) It is suggested that this factor of 1.6 be applied as a normalization constant to the energy densities obtained from the HI-STORM explosive attack scenario. This will reduce the energies in the homogeneous model used in the simulations to values appropriate for fuel pellets in explicit form.

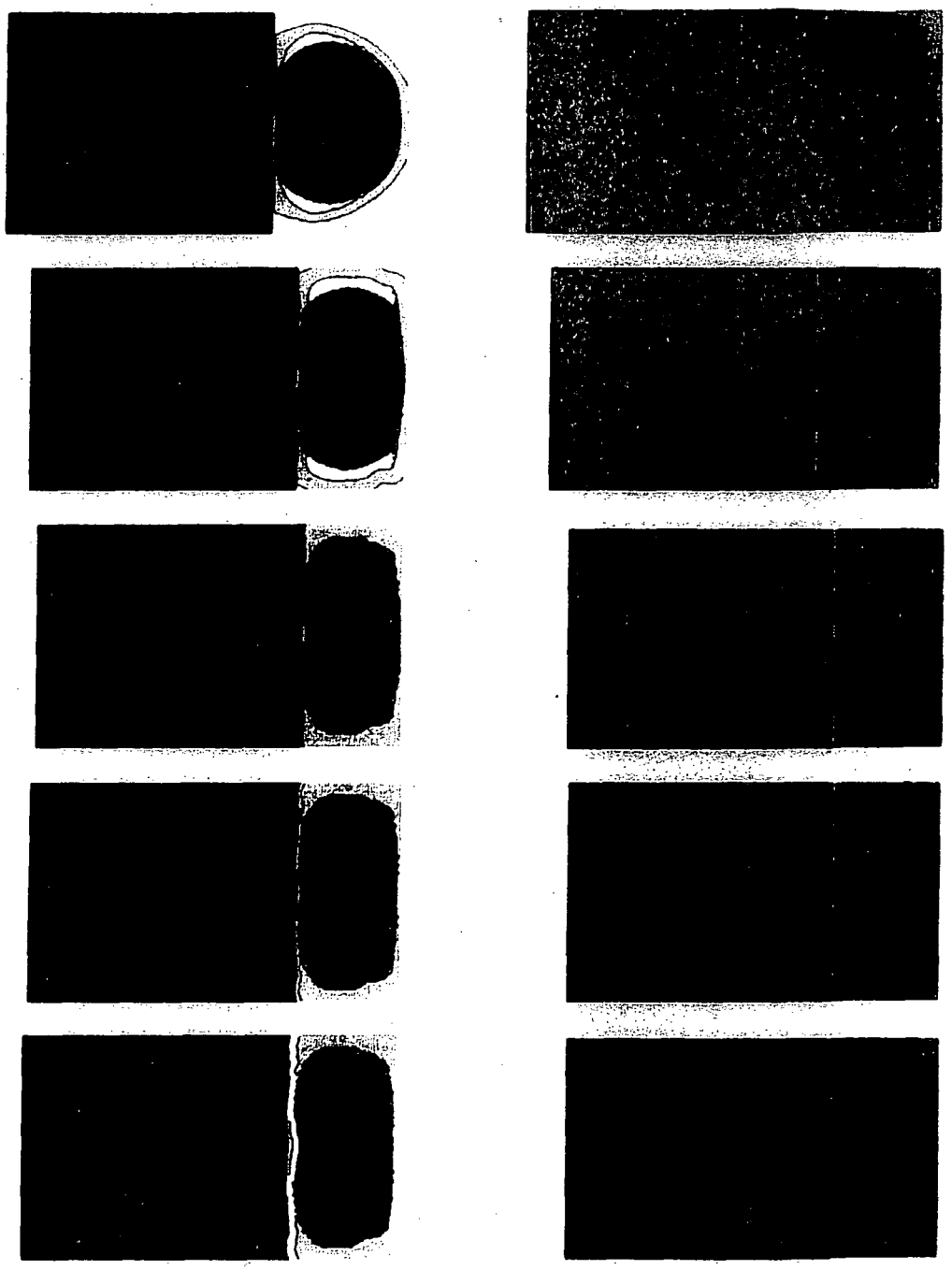

Figure C-2. [The corresponding steel slug / homogeneous fuel is shown on the right. Image times: 20, 40, 60, 80,100 μs (U).
The contents of this figure are unclassified.

ex. 2
p. C-3a

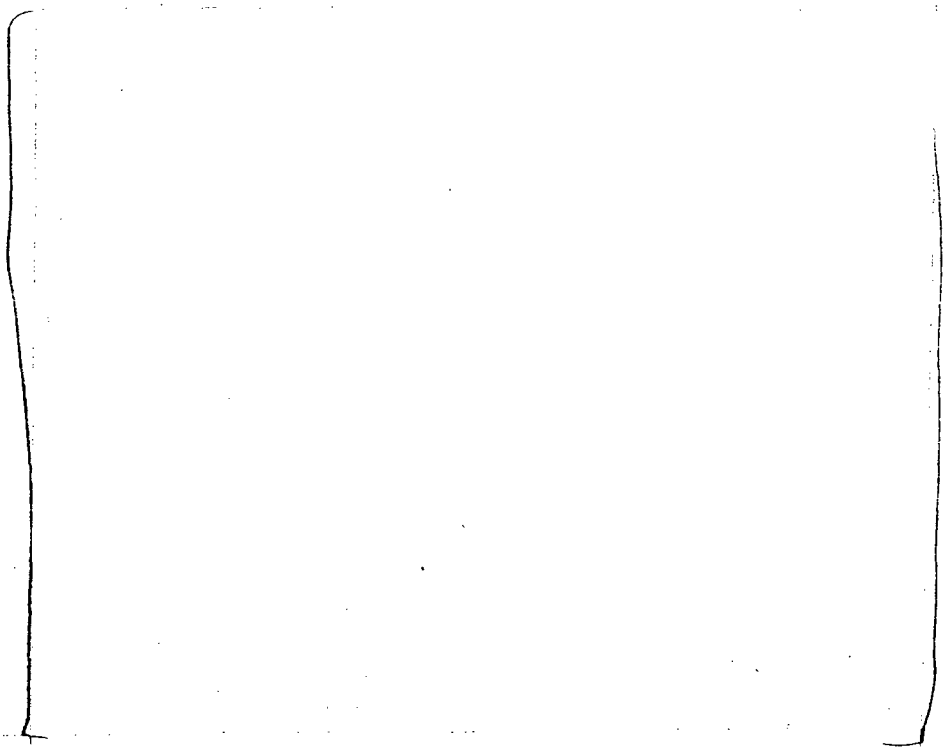

ex. 2
p. C-4a

Figure C-3. Average fuel energy density for both explicit and homogeneous cases (1 J/g = 0.430 BTU/lb) (U).
The contents of this figure are unclassified.

C.2 Single-Pellet Impact (Un-Clad) – Energy Partitioning (U)

(U) When the steel slug impacts the pellet, the initial kinetic energy of the slug is partitioned into internal energy in the pellet, as well as residual internal and kinetic energy of the system.

ex. 2
p. C-4b

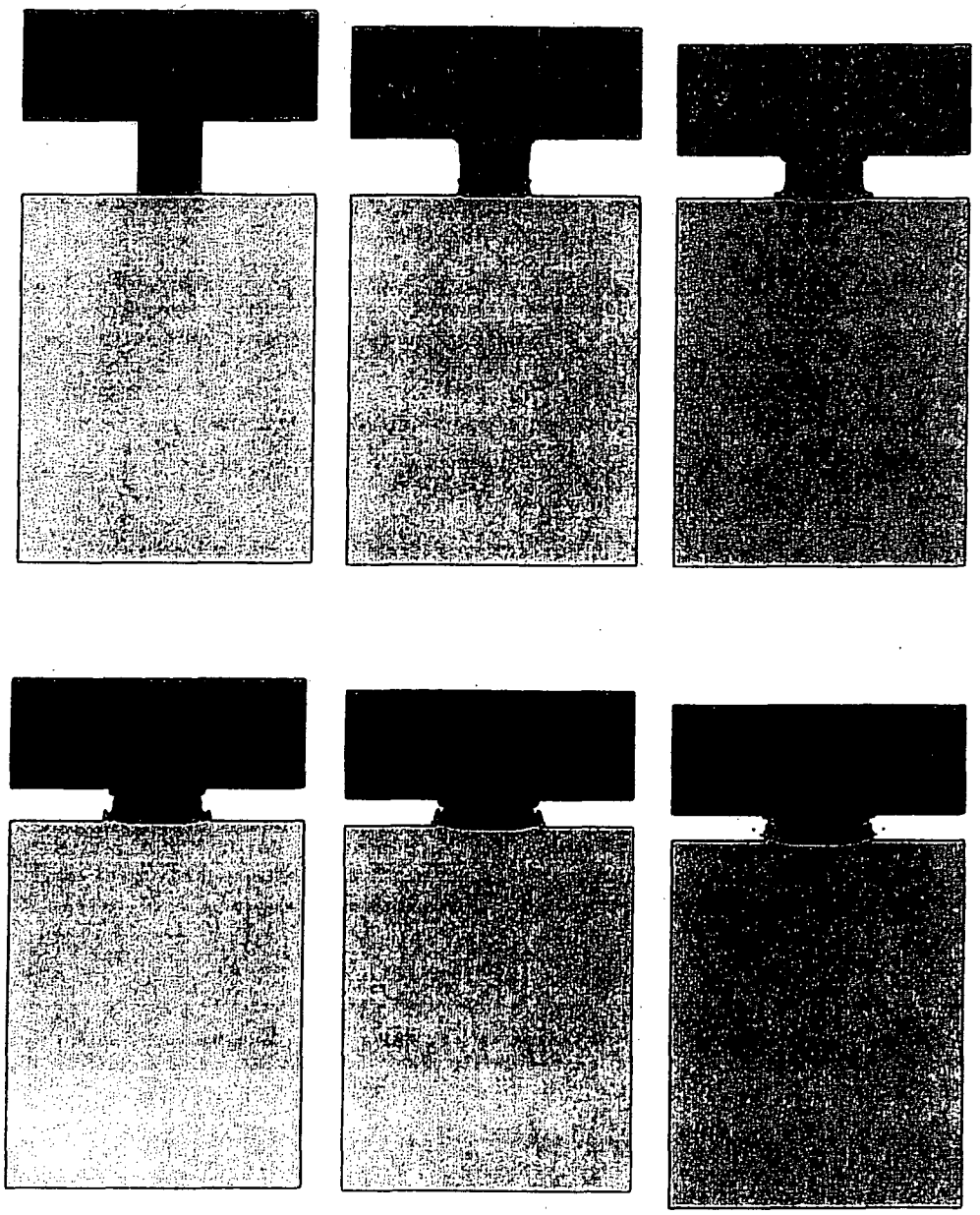

Figure C-4. [

]

Image times: 0, 50, 100, 150, 200,400 μs (U).
The contents of this figure are unclassified.

ex 2
p. C-5a

ox. 2
p. C-6a

Figure C-5. Histories of the kinetic energy loss in the steel impactor and the internal energy gained in the UO_2 pellet (1 J = 0.737 ft-lb) (U).
The contents of this figure are unclassified.

Appendix D

Appendix D: Sample CTH Input File (U)

Ex # 2
P.D-12

$\mathcal{E}_x = 2$ p. D-3a

Ex # 2 p. D-4a

Ex # 2 P. D-5a

Ex # 2 p. D-7a

Ex #2 p.D-8a

Ex # 2 p.D-10a

Ex "2" p.D-12a

Ex # 2 p. D-14a